AD-A179 499 CONTINUATION OF RESEARCH IN THE DEVELOPMENT OF HIGH SENSITIVITY X-RAY AND (U) CALIFORNIA UNIV BERKELEY ELECTRONICS RESEARCH LAB A BELL ET AL 25 FEB 87 1/2

UNCLASSIFIED AFOSR-TR-87-0380 AFOSR-85-0084 F/G 13/8 NL

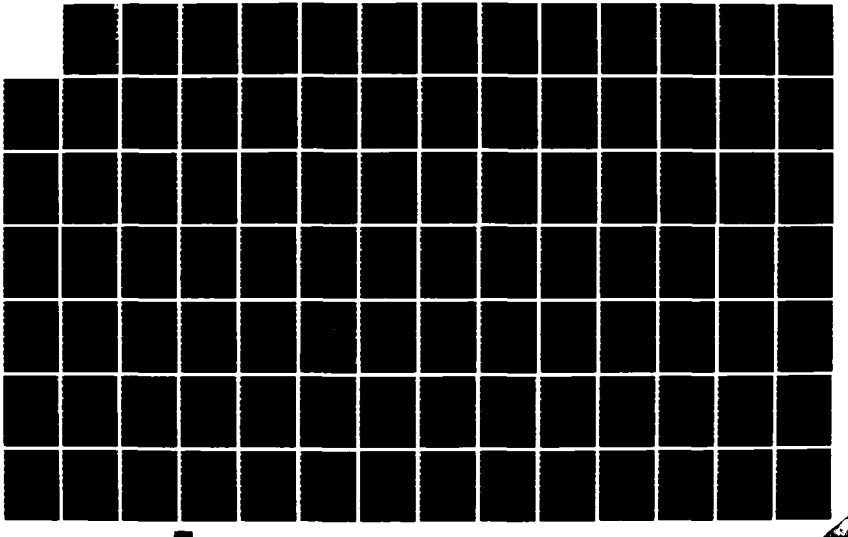

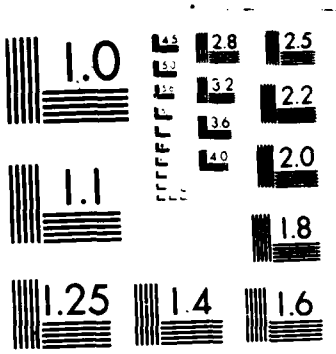

AFOSR-TR- 87-0380

CONTINUATION OF RESEARCH IN THE DEVELOPMENT OF HIGH SENSITIVITY X-RAY AND ELECTRON BEAM RESISTS PROCESSES

Final Technical Report
AFOSR Grant 85-0084
(January 1, 1985 - June 30, 1986)

Alexis Bell, Dennis Hess, David Soong
Co-Principal Investigators

Department of Electrical Engineering and Computer Sciences
and the Electronics Research Laboratory
University of California
Berkeley, CA 94720

SECURITY CLASSIFICATION OF THIS PAGE

REPORT DOCUMENTATION PAGE

1a. REPORT SECURITY CLASSIFICATION Unclassified	1b. RESTRICTIVE MARKINGS
2a. SECURITY CLASSIFICATION AUTHORITY	3. DISTRIBUTION / AVAILABILITY OF REPORT Unlimited
2b. DECLASSIFICATION / DOWNGRADING SCHEDULE	
4. PERFORMING ORGANIZATION REPORT NUMBER(S)	5. MONITORING ORGANIZATION REPORT NUMBER(S) **AFOSR-TR- 87-0380**
6a. NAME OF PERFORMING ORGANIZATION Electronics Research Lab. / 6b. OFFICE SYMBOL (If applicable)	7a. NAME OF MONITORING ORGANIZATION Air Force Office of Scientific Research
6c. ADDRESS (City, State, and ZIP Code) University of California Berkeley, CA 94720	7b. ADDRESS (City, State, and ZIP Code) Bldg. 410, Bolling Air Force Base Washington, DC 20332
8a. NAME OF FUNDING / SPONSORING ORGANIZATION AFOSR / 8b. OFFICE SYMBOL (If applicable) NE	9. PROCUREMENT INSTRUMENT IDENTIFICATION NUMBER AFOSR-85-0084
8c. ADDRESS (City, State, and ZIP Code) Bldg 410 B.A.F.B. D.C. 20332-6448	10. SOURCE OF FUNDING NUMBERS PROGRAM ELEMENT NO. 61102F / PROJECT NO. 2306 / TASK NO. B2 / WORK UNIT ACCESSION NO.

11. TITLE (Include Security Classification)
Continuation of Research in the Development of High Sensitivity X-ray and Electron Beam Resists Processes

12. PERSONAL AUTHOR(S)
Alexis Bell, Dennis Hess, David Soong

13a. TYPE OF REPORT	13b. TIME COVERED	14. DATE OF REPORT (Year, Month, Day)	15. PAGE COUNT
Final Report	FROM 1/1/85 TO 6/30/86	2/25/87	

16. SUPPLEMENTARY NOTATION

17. COSATI CODES			18. SUBJECT TERMS (Continue on reverse if necessary and identify by block number)
FIELD	GROUP	SUB-GROUP	

19. ABSTRACT (Continue on reverse if necessary and identify by block number)

Electron-beam lithography is used for mask making, and offers promise for fabrication of high density integrated circuits since it does not have the inherent limitations of optical lithography. Investigations were conducted under AFOSR Grant 85-0084 to obtain a better understanding of e-beam resist dissolution with a direct application to the image transfer step in e-beam lithography. Studies were performed with poly(methyl methacrylate), PMMA, which is a commonly used electron beam resist. The studies included the monitoring of resist swelling and dissolution kinetics using in-situ ellipsometry, and modeling efforts to describe the basic physcs of resist dissolution.

20. DISTRIBUTION / AVAILABILITY OF ABSTRACT	21. ABSTRACT SECURITY CLASSIFICATION	
☒ UNCLASSIFIED/UNLIMITED ☐ SAME AS RPT. ☐ DTIC USERS		
22a. NAME OF RESPONSIBLE INDIVIDUAL	22b. TELEPHONE (Include Area Code)	22c. OFFICE SYMBOL

ABSTRACT

Electron-beam lithography is used for mask making, and offers promise for fabrication of high density integrated circuits since it does not have the inherent limitations of optical lithography. Investigations were conducted under AFOSR Grant 85-0084 to obtain a better understanding of e-beam resist dissolution with a direct application to the image transfer step in e-beam lithography. Studies were performed with poly(methyl methacrylate), PMMA, which is a commonly used electron beam resist. The studies included the monitoring of resist swelling and dissolution kinetics using in-situ ellipsometry, and modeling efforts to describe the basic physics of resist dissolution.

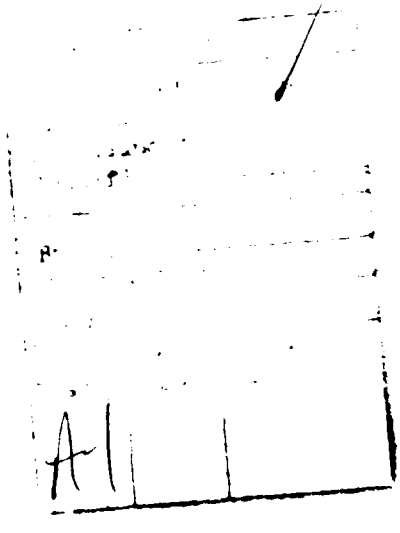

INTRODUCTION

Investigations were performed under AFOSR Grant 85-0084 to study the swelling and dissolution behavior of electron beam resists. These studies concentrated on poly(methyl methacrylate), PMMA, since it is a common e-beam resist, and the material properties of this polymer have been extensively researched. The studies included monitoring swelling and dissolution of PMMA films using in-situ ellipsometry, and modeling of swelling and dissolution based on transport and polymer physics. This report summarizes the accomplishments to date. The experimental portions of the work are presented first, followed by the theoretical aspects of the work.

SWELLING AND DISSOLUTION STUDIES

Summary

The swelling and dissolution of thin film poly(methyl methacrylate), PMMA, in methyl isobutyl ketone (MIBK), and in solvent/nonsolvent mixtures of MIBK/methanol and methyl ethyl ketone/isopropanol have been investigated. Films were monitored using *in situ* ellipsometry. Parametric studies of the effects of molecular weight, molecular weight distribution, softbake quench rate, solvent size, and temperature were performed with MIBK. These parameters were shown to have a significant effect on dissolution. The effects of solvent composition and temperature on swelling and dissolution were investigated with the binary solvents. Ternary diagrams based on Flory-Huggins interaction parameters were used to interpret the thermodynamics of swelling and dissolution. A narrow transition region (NTR)

where the developer changed from a swelling to dissolving agent with a small change in composition or temperature was observed.

Background

Few systematic studies on the effect of molecular weight distribution (MWD), softbake cooling rate, sample aging, and dissolution temperature on resist development have been reported. The MW effect on PMMA dissolution has been investigated previously[1-3], but these studies have often shown dissimilar behavior for the dissolution rate dependence on MW. The effect of MWD on sensitivity and contrast has been reported[4-6], but no direct studies have been performed to compare dissolution rates of samples with different MWD's. It has been reported[7] that the rate at which thick (1 mm) samples of PMMA were cooled through the glass transition temperature (T_g) affected the rate of methanol absorption. This effect is believed to be due to the 'freezing-in' of excessive free volume at higher cooling rates. The more free volume present in a polymer, the greater the solvent penetration rate. Polymers are also known to undergo volume relaxation, whereby the trapped-in free volume decreases and approaches its equilibrium state with time[8].

Resist development often involves the use of binary solvent mixtures which consist of a strong solvent and a moderating nonsolvent[9]. The effects these solvent/nonsolvent developers exert on the swelling and dissolution behavior of resists are complex and their interpretation has generally been accomplished by noting the topographical profiles of the developed images. A systematic <u>in situ</u> study of simultaneous dissolution and swelling of resists in solvent mixtures can provide insight into the complex mechanisms of the

development process.

During development, solvent penetration and resist dissolution are controlled by kinetic and thermodynamic solvent/polymer interactions. In general, solvent mobility is primarily related to its molecular size whereas thermodynamic compatibility is associated with the strength of the interactions between structural groups of both polymer and solvent molecules. An approximate measure of thermodynamic compatibility is given by the solubility parameter, δ[10,11]. Another measure of polymer-solvent compatibility is given by the Flory-Huggins interaction parameter, χ_{ij}, where the subscripts refer to pair interactions in multi-component systems[12]. Values of χ_{ij} for some polymer-solvent systems can either be found in the literature[13] or roughly calculated from solubility parameters[14]. Unfortunately, tabulated values for polymer solubility parameters can range widely and data for χ_{ij} are somewhat limited.

Diffusion in glassy polymers is often characterized by a sharp front which penetrates at a constant velocity. This non-Fickian behavior, termed Case II diffusion[15], is controlled by polymer relaxation. For nonsolvent penetration, the thickness of the swollen layer behind the front increases linearly with time. In the case of strong solvents, the gel layer rapidly dissolves into the solvent and its thickness is typically not detectable. Thus with strong solvents, Case II diffusion gives rise to a constant dissolution rate[16]. These two limiting cases of total gel conversion in nonsolvent mixtures and 'immeasurable' gel formation in strong solvents are presented to illustrate the extremes in expected behavior.

In the first part of this experimental study, dissolution rates of poly(methyl methacrylate),PMMA, in methyl isobutyl ketone, MIBK, were investigated. To ascertain the effect of MW on dissolution rate, commercial MW standards of known dispersity were used. After softbaking, samples were cooled at different rates to determine the effect of cooling rate. Then selected samples were aged at room temperature and at 60°C to determine the effect of aging. (All data presented in this paper are for unexposed PMMA.) Finally, apparent activation energies were obtained for different molecular weight dispersity and softbake cooling rates to determine how these factors affect the temperature sensitivity of dissolution.

For the second part of this study, binary systems of methyl ethyl ketone(MEK)/methanol(MeOH) and MIBK/isopropanol(IpOH) were used. Based on solubility parameters, MEK and MIBK are solvents for PMMA, whereas the alcohols are nonsolvents. The effects of temperature and solvent/nonsolvent composition on dissolution and swelling were examined.

Experimental

Rate Measurement

A modified version of the psi-meter described earlier[17] was used for in situ monitoring of dissolution and swelling. A psi-meter is a single-element rotating-polarizer ellipsometer in which an incident laser beam is polarization modulated and the intensity fluctuation of the reflected light measured. The ratio of the AC and DC components of the reflected intensity is related to the optical parameter psi (ψ) by $AC/DC=-\cos 2\psi$ [18]. To determine film thickness as a function of time, calculated values of ψ or

AC/DC are compared to experimental data. Theoretical data were produced using an ellipsometry program[19] which requires input of the laser wavelength and angle of incidence, the refractive indices of the substrate, film, and immersion medium, and the thicknesses of the glassy and swollen layers. For this study, the angle of incidence was 75° and the wavelength was 632.8 nm (2mW He-Ne laser). An Abbe refractometer was used to correlate the mixture refractive index with the composition of MEK/IpOH and MIBK/MeOH binary developers. Values of ψ (or equivalently AC/DC) were collected continuously during dissolution at a rate of one point per second.

Materials

Commercial PMMA standards of known MWD (see Table 1) were obtained from Polysciences, Inc. PMMA standards were dissolved in chlorobenzene to a concentration of approximately 8 volume percent. In addition, a polydisperse (M_n=180,000; M_w/M_n=2.8) PMMA electron-beam resist (6 weight percent in chlorobenzene) was obtained from KTI Chemicals, Inc. The molecular weight distribution of the KTI resist was determined by gel permeation chromatography[20].

Procedures

The PMMA solutions were spin-coated onto silicon wafers at approximately 1500-2000 RPM. Samples were softbaked at 160°C for one hour in a nitrogen purged, convection oven and then cooled gradually inside the oven or quenched in either liquid nitrogen or ambient. The cooling rate through T_g for the slowly cooled samples was approximated as 0.8°C/min by monitoring the oven temperature. Thickness measurements of the softbaked films were made with a

Sloan Dektak Profilometer, an Applied Materials AME-500 Manual Ellipsometer, or a Nanometrics Nanospec AFT. Typical thicknesses were in the range 0.65-1.2 μm. For aging studies, one wafer for each of the cooling rates was broken into pieces with approximate areas of 2 cm^2. Half of these pieces were placed inside a nitrogen purged, light filtered glove box at room temperature; the other half were placed inside a nitrogen purged, convection oven maintained at 60°C.

Developer solutions were circulated through an optical cell at about 25 ml/min. This gave an inlet velocity of 80 cm/min and an average channel velocity of 5.2 cm/min based on the inlet tubing and cell cross sectional areas, respectively. Above 25 ml/min, turbulence resulted which caused significant fluctuations in the optical signal. Reducing the flow rate below 25 ml/min did not alter the dissolution rates, suggesting external mass transfer limitations to be relatively unimportant under such operating conditions. The cell temperature was maintained to $\pm$0.1°C with a Yellow Springs Instrument Co., Inc, Model 72 Proportional Temperature Controller.

Results and Discussion

Dissolution in MIBK

A constant dissolution rate and a negligible surface swollen layer were observed for all MIBK studies. This suggests, as discussed earlier, that penetration occurred by Case II transport, and that gel dissolution was rapid relative to solvent penetration.

Temperature Effect. Figure 1 shows the effect of temperature on the

dissolution of air quenched, monodisperse (M_w/M_n<1.11) PMMA. The apparent activation energies, E_a's, are nearly the same for the two molecular weights, indicating that E_a is not a strong function of molecular weight for monodisperse PMMA. The average value of 27 kcal/mol is in good agreement with the value of 24 kcal/mol obtained previously[3]. These relatively high activation energies are indicative of Case II penetration[7].

The effect of temperature on the dissolution of polydisperse KTI PMMA resist for different softbake cooling rates is presented in Figure 2. The rather high E_a of 43 kcal/mol for the slowly cooled KTI resist indicates strong temperature sensitivity for dissolution. A change in temperature of only 1°C in the vicinity of 25°C can affect the dissolution rate by over 25%. The E_a of a slowly cooled KTI resist is 40% greater than that of an air quenched KTI resist and nearly 60% greater than that of an air quenched, monodisperse sample (Fig 1). This wide range in apparent activation energies due to different cooling rates demonstrates the importance of sample handling after softbaking. At a given temperature, the dissolution rate is highest for the sample that underwent the fastest cooling rate (i.e. liquid nitrogen quench) and lowest for the slowest cooling rate.

Molecular Weight Effect. Variation of dissolution rate with molecular weight can be described, at least over a moderate range, by the expression[3,21]:

$$R_d = k\, M^{-A} \qquad [1]$$

where: R_d = dissolution rate
M = molecular weight
A,k = constants

The dissolution rates observed in this study are plotted as a function of M_n and M_w for mono- and polydisperse PMMA in Figure 3. The data are consistent with behavior predicted by Eqn 1. The value of the MW exponent, A, is 0.98. Previous authors[1,3] have observed a non-linear log-log dependence on MW, since a larger MW range was studied than in this work.

Figure 3 also shows that at a given M_n or M_w, the dissolution rate of a polydisperse sample is higher than that of a monodisperse sample. This effect is believed to be due to the wider MWD of polydisperse samples. Shorter chains dissolve at a faster rate than longer chains according to Eqn 1 and, after their removal, allow facile penetration of the polymer by solvent which improves the mobility of the longer chains. This effect enhances the overall dissolution rate of the polydisperse polymer relative to a monodisperse polymer of the same M_n.

The dissolution of air quenched, monodisperse PMMA was carried out at several temperatures and the results are presented in Figure 4. It can be seen that A is independent of temperature, which agrees with previous observations[3,21].

Figure 5 shows the effect of cooling rate on A for monodisperse PMMA samples. If a resist sample is slow cooled instead of air quenched, A can be increased to 1.8. Since a larger A gives a greater difference in solubility rate between exposed and unexposed regions of the resist, slowly cooling a resist after softbaking may enhance the contrast. While this conclusion is based on data for a limited molecular weight range, it suggests greater attention be given to the softbake cooling rate.

Aging Effect. Figure 6 shows the aging effect on the dissolution of polydisperse KTI resist for different cooling rates. Samples were aged at room temperature or at 60°C as indicated. There was no apparent change in the dissolution rate for samples aged at room temperature over a period of 100 hours. Also, samples that were cooled slowly after softbaking showed no significant change in the dissolution rate for the same aging period. However, the liquid nitrogen and air quenched samples which were aged at 60°C showed a noticeable decrease in the dissolution rate after the first 24 hours and a gradual decrease thereafter. These observations can be explained in terms of changes in the polymer free volume.

The greater the rate at which a polymer is cooled through T_g, the greater the amount of free volume 'frozen-in'. In time, the polymer chains relax and the free volume fraction decreases toward its equilibrium state of 0.025[8]. For samples cooled gradually after softbaking, it appears the polymer has adequate time to closely establish its equilibrium free volume. Hence, aging these samples exerts a negligible effect on their dissolution rate. The liquid nitrogen and air quenched samples displayed a relaxation effect due to aging at 60°C (Fig 6) With sufficient time, these quenched samples would be expected to approach the equilibrium free volume and, hence, dissolve at a comparable rate to slowly cooled ones. The samples aged at room temperature show no change in dissolution rate, but the relaxation rate is probably so slow that the effect on dissolution is negligible. With sufficient aging, these samples would also be expected to show a decrease in dissolution rate.

Swelling and Dissolution in Solvent/Nonsolvent Mixtures

MEK/IpOH - Composition Effect. For a 1.2 μm PMMA film immersed in 40:60 MEK/IpOH at 24.8°C, less than 2% of the PMMA dissolved. However, in 80:20 MEK/IpOH at the same temperature, the sample dissolved in about four minutes. The dissolution was linear with negligible gel layer formation. These two solvent compositions yield two distinctly different solubility regimes - pure swelling and complete dissolution. The transition between these regimes was observed over a narrow concentration range. For MEK/IpOH at 24.8°C, this narrow transition range (NTR) occurred from 45:55 to 50:50 MEK/IpOH. Since it has been shown[5] that polymer solubility decreases with increasing MW and decreasing temperature, the width and position of this NTR would be expected to be functions of both temperature and polymer MW. To illustrate these effects, ternary phase diagrams were constructed from polymer phase equilibria theory for different MW's and temperatures.

Phase Equilibria. From the Flory interaction parameters (χ_{ij}) and the molar volumes (v_i) of nonsolvent, solvent and polymer, a binodal curve of a ternary phase diagram can be constructed by equating the chemical potentials (μ_i) in both phases for each component i. Equations for μ_i in terms of χ_{ij} and v_i are available[12]. Figure 7 is a ternary phase diagram for a nonsolvent(1), solvent(2), polymer(3) system for $\chi_{23}=0$, $\chi_{12}=\chi_{13}=1$, $v_1=v_2=100$ cm^3/mol and polymer MW = 2×10^5. The selected χ_{ij}'s are approximate values for the IpOH/MEK/PMMA system calculated from solubility parameters. The chosen MW is the measured M_n of the KTI resist.

In Figure 7, points A and B correspond to two hypothetical overall

compositions representative of our operating conditions, i.e. polymer fractions of about 10^{-5}. Point A lies within the single phase region, and hence, the resist material dissolves completely into the developer solution (as was seen for 80:20 MEK/IpOH). Point B lies within the two phase region. Although not discernible in Figure 7, the calculated polymer fraction in the polymer-poor phase is much less than 10^{-5}. Therefore, this phase would consist overwhelmingly of nonsolvent and solvent. The other phase in equilibrium with B has a composition represented by point B' (located via the tie line). This implies that at a developer composition given by point B, the resist would not dissolve but, instead, would absorb solvent and nonsolvent from the developer solution until the equilibrium swollen gel composition given by B' is reached. When the developer composition lies near the binodal curve, complex dissolution behavior is expected. Slight changes in MW, composition, or temperature could effectively shift the developer from the one phase to the two phase region, or vice versa,, giving rise to the observed NTR. The above discussion assumes monodisperse polymer. For polydisperse polymer, a family of binodal curves will be applicable, and the NTR will be broadened.

MEK/IpOH - Temperature Effect. KTI resist samples were immersed in 50:50 MEK/IpOH at 24.8°C, 21.7°C and 18.4°C. At 24.8°C, the resist dissolved completely. At 21.7°C, however, 15% of the resist was found to be insoluble and, at 18.4°C, as much as 65% was insoluble. The incomplete dissolution was most likely due to the relatively broad MWD of the KTI resist and suggests that the resist material was undergoing MW fractionation due to the relative solubilities of the higher and lower molecular weight polymer chains. For a

solvent with marginal dissolution capabilities (e.g., 50:50 MEK/IpOH), a decrease in dissolution temperature will cause a greater proportion of the higher MW chains to become insoluble.

The AC/DC data for the lower temperatures indicated that initially Case II swelling was occurring, and partial dissolution followed. Apparently, in the initial stages of penetration, diffusion of the lower MW polymer chains is hindered by the presence of the insoluble higher MW chains so relatively little dissolution can occur and therefore, swelling becomes the primary effect observed. After the polymer swells to a sufficient extent, mobility of the shorter chains is increased. These shorter chains can then migrate to the surface and diffuse into the solvent.

MIBK/MeOH - Composition Effect. Experiments similar to those described for MEK/IpOH were performed with MIBK/MeOH. At 24.8°C, 40:60 MIBK/MeOH showed virtually no dissolution, whereas 75:25 MIBK/MeOH dissolved totally. The NTR occurred between 40:60 and 50:50 MIBK/MeOH which is similar to the NTR found for MEK/IpOH.

Summary of Kinetics. Figure 8 summarizes the effect of solvent composition on the penetration and dissolution rates of PMMA for MEK/IpOH and MIBK/MeOH at 24.8°C. For MEK/IpOH (Fig 8a), the penetration rate rises gradually from zero at 100% IpOH to about 70 nm/min at the NTR. Above the NTR the penetration rate rises more rapidly to an upper limit of 410 nm/min. There is essentially no dissolution until the NTR is reached. In the NTR, dissolution rate rises rapidly and becomes equal to the penetration rate. The region enclosed by these two curves represents the solvent composition

range in which considerable gel growth is encountered.

MIBK/MeOH (Fig 8b) displays somewhat different kinetic behavior. The penetration rate of the nonsolvent is appreciable. This difference is due to the smaller size of the MeOH molecule relative to IpOH. The dissolution and penetration rates reach a maximum just above NTR and decrease above about 75% MIBK with pure solvent (100% MIBK) actually yielding the slowest penetration rate. Hence, it can not be assumed that increasing the nonsolvent concentration in the developer solution would necessarily reduce the dissolution rate. Enhancement of penetration rates due to the presence of kinetically mobile species has been observed previously[16].

Summary of Thermodynamics. The effect of developer composition on thermodynamic behavior could be summarized most effectively by representing equilibrium data in a ternary phase diagram. Unfortunately, the psi-meter is incapable of distinguishing the individual concentrations of solvent and nonsolvent in the swollen gel, for it 'sees' only their combined swelling effect. However, swelling can be described in terms of the gel layer polymer fraction, P^*. Alternately, a swelling factor, S, can be defined as the ratio of gel thickness at equilibrium (h^*) to initial resist thickness (h_o). Assuming the volumes of polymer, solvent and nonsolvent are ideally additive and no polymer dissolves, S is simply the reciprocal of P^*.

$$S = \frac{h^*}{h_o} = \frac{1}{P^*} \qquad [2]$$

Figure 9 summarizes the effect of developer composition on resist swelling and solubility for MEK/IpOH and MIBK/MeOH. For MEK/IpOH (Fig 9a), S rises

almost linearly from a value of one (no swelling) at 100% IpOH to about three at the NTR. Above the NTR, S = 0 since all the polymer dissolves at equilibrium. MIBK/MeOH (Fig 9b) shows a similar trend with S rising from 1.4 at 100% MeOH to about 3 at the NTR. Figure 9 suggests that for a given developer composition near the NTR in the one phase region, a slight decrease in the developer strength, decrease in temperature, or increase in resist MW may bring about sizable swelling of the resist. In addition, S reaches its maximum value in the NTR, indicating that when this region is crossed, the effect of swelling can be most severe.

Conclusions

These studies have demonstrated the usefulness of <u>in situ</u> ellipsometry for monitoring resist swelling and dissolution. They have also shown that softbake cooling rate and molecular weight dispersity can significantly affect dissolution. The effective activation energy, E_a and the molecular weight exponent, A, were found to vary by as much as 85% depending on the cooling rate. In particular, A was 0.98 for air quenched and 1.8 for slowly cooled monodisperse polymer samples. Also, aging at 60°C lowered the dissolution rates of rapidly quenched samples by about 25%. PMMA of broad MWD was found to dissolve at a faster rate than monodisperse samples of the same M_n.

A thermodynamically controlled NTR between swelling and dissolution regimes was observed with MEK/IpOH and MIBK/MeOH mixtures. At 24.8°C, the transition occurred near 50:50 solvent/nonsolvent for with both mixtures. At this composition, a decrease in temperature reduced the amount of polymer

dissolved. Incomplete dissolution was believed to be due to fractionation which yielded an insoluble film of higher MW than the original material. Usually, a period of initial swelling was followed by partial dissolution. This induction period was attributed to hindered diffusion of the soluble, shorter polymer chains due to the presence of insoluble, longer chains.

Synergistic effects were also observed with MIBK/MeOH mixtures. For the MEK/IPOH system the penetration rate was found to increase with increasing solvent to nonsolvent ratios. However, for MIBK/MeOH, a maximum in penetration rate was observed for an intermediate composition of about 75:25 MIBK/MeOH. This effect was probably due to the ability of the relatively small MeOH molecule to penetrate and 'open-up' the polymer network.

The experimental work summarized here led to the submission of two papers for publication. Copies of these two papers are included in the appendix of this report.

MODELING

Summary

Fundamental models were developed to describe the swelling and dissolution of thin polymer films. These models account for solvent penetration by Fickian and Case II transport. Chain disentanglement is treated using reptation concepts. To date, these models have been developed and implemented on an IBM 3090 computer for numerical solution. Parametric simulations are currently underway.

Background

The objective of the theoretical work was to develop models for swelling and dissolution of thin film polymers based on fundamental transport equations and polymer physics. The dissolution process consists of several basic steps. First, the solvent molecules must penetrate into the glassy matrix, causing local swelling and increasing the mobility of the polymer chains. Once the glassy matrix is converted into a swollen, somewhat rubbery material, which will be referred to as the "gel", the polymer chains can disentangle from the other chains. If disentanglement occurs very slowly or not at all, then only swelling of the film will be observed. The freed chains must then diffuse into the bulk solvent.

A fundamental model for resist dissolution where penetration occurs by Fickian diffusion has been reported[22]. The surface disentanglement term was set equal to a constant, and no theoretical expression was given for this rate. Further, solvent penetration in many glassy polymers occurs by Case II transport, so a dissolution model for Case II penetration is needed. It should be noted that a single model to span both penetration modes is not feasible, so a different model for each mode is necessary. Several models have been proposed to describe Case II swelling in the absence of dissolution. Some of these approaches have modified the diffusivity to be concentration, stress, or time dependent[23,24]. Two significantly different approaches have also been reported. One of these[25] is based on the viscous response of the polymer to the osmotic pressure developed by the presence of the penetrating solvent. Activity profiles and strain of the polymer due to

the viscous response are solved simultaneously. The second model[26] is based on the phenomenological similarity of penetration to crazing behavior. The penetration of the sharp front is given by a kinetic expression which is proportional to the difference between the stress level in the film and the critical stress for crazing. The diffusion equation is solved behind the front to determine the solvent concentration profile. Since both of these models were developed for purely swelling cases, neither accounts for dissolution.

The disentanglement rate of polymer chains is expected to depend on the molecular weight and concentration of the polymer. This aspect of the dissolution process has not been fundamentally addressed in the literature. However, the physics of disentanglement can be treated in terms of reptation theory[27], as will be discussed later. The rate at which the disentangled chains are transported into the bulk solvent will depend on the diffusivity of the polymer chains in solution, and the solvent flow rate.

The contributions of this work are the inclusion of surface disentanglement into the Fickian and Case II penetration models, and a formulation of the gel-solvent interface (GSI) concentration for dissolution based on entanglement energetics. To date, the models have been developed and implemented on an IBM 3090 computer, but parametric simulations are not complete. Thus, the development of the equations will be presented, but results will be reported later[28].

Fickian Penetration

The Fickian model described here is equivalent to the one noted earlier[22]. It is a dimensional model that has one moving boundary, the GSI. Figure 10a shows the coordinate system. The frame of reference is fixed with respect to the laboratory. The local mass flux of solvent in the polymer, j_s, is given by

$$j_s = -D_s(C_s)\partial C_s/\partial x \qquad [3]$$

where D_s is diffusivity, and C_s is the solvent mass concentration. Now

$$C_s = w_s \rho \qquad [4]$$

where w_s is the mass fraction of solvent and ρ is the density of the mixture. If ideal mixing is assumed, then

$$\rho = \sum \phi_i \rho_i \qquad [5]$$

where ϕ_i and ρ_i are the volume fraction and density, respectively, of component i. Also, for the binary solvent(1)/polymer(2) mixture,

$$C_s = x_s = (\phi_1\rho_1+\phi_2\rho_2)\rho_1 V_1/(\rho_1 V_1+\rho_2 V_2) \qquad [6]$$

$$= (\phi_1\rho_1+\phi_2\rho_2)(\rho_1\phi_1)/(\rho_1\phi_1+\rho_2\phi_2) = \rho_1\phi_1$$

Here V_i is the volume of component i in some control volume. Thus the flux can be written,

$$j_s = - D(\phi_1)\rho_1\partial\phi_1/\partial x \qquad [7]$$

A "flux" or diffusive velocity can then be expressed as (dropping subscript),

$$j'_s = - D(\phi)\partial\phi/\partial x \qquad [8]$$

where j'_s equals j_s/ρ_1. This convention is convenient since the problem is one dimensional, and since experimentally thickness and refractive index changes are measured, not mass uptake. The solvent and polymer are assumed to be incompressible, and since mixing is assumed to be ideal (no volume change), the local swelling velocity, v, is given by

$$v=-j'_s = D(\phi)\partial\phi/\partial x \qquad [9]$$

Relative to a stationary observer, the conservation equation for solvent in the polymer film is given by

$$\partial\phi/\partial t =-\partial(j'_s + \phi v)/\partial x=-\partial(-D(\phi)\partial\phi/\partial x+\phi D(\phi)\partial\phi/\partial x)/\partial x \qquad [10]$$

Differentiating and using the chain rule for $\partial D/\partial x$ gives

$$\partial\phi/\partial t = (1-\phi)D(\phi)\partial^2\phi/\partial x^2 + (\partial\phi/\partial x)^2[(1-\phi)dD(\phi)/d\phi-D(\phi)] \qquad [11]$$

Expressing the diffusivity as $D=D_o f(\phi)$, the conservation equation can be written as,

$$\partial\phi/\partial t=(1-\phi)D_o f(\phi)\partial^2\phi/\partial x^2+(\partial\phi/\partial x)^2[(1-\phi)D_o df/d\phi-D_o f(\phi)] \qquad [12]$$

This equation can be made dimensionless by introducing the dimensionless variables,

$$\tau = D_o t/A^2 \qquad \bar{x} = x/A$$

where A is the initial film thickness. Although ϕ is already dimensionless,

one could also define a reduced ϕ relative to some equilibrium solvent fraction, ϕ^*. However, ϕ was used for convenience. Substituting the dimensionless quantities yields

$$\partial\phi/\partial\tau=(1-\phi)f(\phi)\partial^2\phi/\partial\bar{x}^2+(\partial\phi/\partial\bar{x})^2[(1-\phi)df/d\phi-f(\phi)] \qquad [13]$$

The initial condition is solvent free polymer except at the surface, where the immersed sample immediately reaches a surface concentration corresponding to the appropriate boundary condition.

$$\phi(\bar{x},0)=0 \quad 0<\bar{x}<1 \qquad [14]$$

$$\phi(\bar{x}=1,0)=\phi^* \quad \text{swelling}$$
$$=\phi_{dis} \quad \text{dissolution}$$

There are two possible values for the GSI, $\bar{x}=\bar{x}_1$. For pure swelling, the concentration at the polymer surface is given by the equilibrium solvent fraction,

$$\phi(\bar{x}_1,t)=\phi^* \qquad [15]$$

For dissolution, the equilibrium approach is not applicable, since at equilibrium only one phase is not present. However, a pseudo equilibrium can be used if an entanglement energy term is added to the expression for the chemical potential of the solvent. This follows previous theories for polymer networks[12]. Since the chains cannot instantaneously disentangle, there will be a restraining force against additional solvent uptake. The derivations will be reported elsewhere[28]. The second boundary condition is no flux at the substrate,

$$\partial\phi/\partial\bar{x}\Big|_{\bar{x}=0} = 0 \qquad [16]$$

The movement of the polymer-solvent interface is given by,

$$d\bar{x}_1/d\tau = -(A/D_o)(j'_s)\Big|_{\bar{x}_1} = (A/D_o)v\Big|_{\bar{x}_1} \qquad [17]$$

The position can be checked for consistency by summing up the total solvent in the film.

Case II Penetration

Our description of Case II penetration closely follows the stress driven model[26] mentioned earlier. A convective term due to local swelling is included. The solvent concentration in the glassy region ahead of the sharp front is assumed to be zero. As with the Fickian model, this model is one dimensional, but now two moving boundaries must be followed, the gel-glass interface (GGI) and the GSI. These boundaries are shown in Figure 10b.

The kinetics of the penetrating front, $x=x_2$ (or $x=x_2$), are governed by the stress level according to

$$d\bar{x}_2/dt = v_2 = K(\sigma-\sigma_c) \qquad [18]$$

v_2 = penetration velocity

k = front factor = $k_o\exp(-E_a/RT)$
σ = total stress
σ_c = critical stress for crazing = constant*(T_g-T)

The total stress is comprised of several terms

$$\sigma = a(\pi_{eq} + \pi^E) + \sigma_{ds} \qquad [19]$$

a = constant

π_{eq} = equilibrium osmotic stress
π^{E} = excess stress
σ_{ds} = differential swelling stress

The constant, a, converts isotropic pressure to a uniaxial stress, which is more consistent with crazing. The osmotic stress is given by the Flory-Huggins theory[12],

$$\pi_{eq} = RT[\phi-\chi\phi^2-\ln(1-\phi)/X]/V_1 \qquad [20]$$

V_1 = molar volume of the solvent
χ = Flory-Huggins interaction parameter
T = temperature
R = gas constant
$X = V_2/V_1$

The solvent fraction in Eqn 20 is that at the GGI. The residual stress is due to non-equilibrium in the film prior to immersion in the solvent. This results from incomplete annealing and/or rapid quenching of the film. The differential swelling stress is due to the mismatch of the swollen region on top of the unswollen glassy polymer. The swollen layer pulls on the rigid glass, and the glass in turn constrains the swollen gel. Thus the glass is in tension and the gel is in compression. The differential swelling stress is a function of time. It depends on the degree of swelling, relaxation time of the swollen polymer and the thickness of the glass. Stress relaxation in the swollen region can be modeled by a Maxwell type equation. The tension arising from differential swelling stress effectively opens up the glassy matrix and facilitates solvent penetration. For the initial studies, only the osmotic stress term is being considered.

Behind the penetrating front, the Fickian diffusion equation,

$$\partial\phi/\partial\tau = (1-\phi)f(\phi)\partial^2\phi/\partial\bar{x}^2 + (\partial\phi/\partial\bar{x})^2[(1-\phi)df/d\phi - f(\phi)] \qquad [13]$$

is solved. The initial condition is also the same as the Fickian model - solvent free polymer except at the polymer surface. The boundary condition at the GSI, a fixed concentration set by equilibrium or entanglement modified equilibrium, is also identical to the Fickian model. The other boundary condition differs, however. At the GGI, the convective flux due to penetration must be matched by the diffusion flux in the gel at the interface. The boundary condition here is,

$$\partial\phi/\partial x = (A/D_o)v\phi/((1-\phi)f(\phi)) = (\partial\phi/\partial x)\phi/((1-\phi)f(\phi)) \qquad [21]$$

Also, while the diffusion equation is solved in the entire polymer for the Fickian case, it is solved only in the penetrated region of the polymer in the Case II situation.

Surface Disentanglement

Once penetrated, the polymer chains will disentangle if the solvent is thermodynamically favorable. The dissolution rate will be dependent on how rapidly the chains can disentangle. A model has been developed[27] for the dynamics of entangled polymer chains, which is referred to as reptation theory. Our approach is to apply reptation theory to predict how disentanglement rate scales with polymer molecular weight and concentration.

As a starting point, the disentanglement rate is proportional to some characteristic length divided by a characteristic time. The thickness of a monolayer was chosen as the characteristic length, and the reptation time constant was chosen as the characteristic time. The monolayer thickness can

be approximated by the radius of gyration of the polymer molecule. Thus, the disentanglement rate will be proportional to,

$$\text{rate} \sim \frac{\text{radius of gyration}}{\text{reptation time}}$$

It can be shown that this ratio leads to the following form for the disentanglement rate,

$$\text{rate} = K/(M^{2.5}(1-\phi)^{1.625}) \qquad [21]$$

where K is a constant that must be derived empirically. The molecular weight exponent can be tested experimentally by looking at monodisperse dissolution for disentanglement limited cases. To include dissolution, the GSI movement equation, Eqn 17, which applies for both Fickian and Case II penetration, is modified to

$$d\bar{x}/d\tau = -\partial\phi/\partial\bar{x} - \bar{R} \qquad [22]$$

where $\bar{R}$ is the dimensionless dissolution velocity. For pure swelling the surface attrition term, $\bar{R}$, is set to zero.

Solution Techniques

The differential equations are solved using a Crank-Nicholson implicit finite difference technique. The one dimensional geometry gives a tridiagonal matrix, which simplifies the computations. Matrix elements for the bulk of the film are straightforward, but points near the moving boundaries require special attention. In brief, the interface locations are tracked using front-following techniques[29]. A fixed grid is used, so often

the interfaces are between grid points. Modified expressions for the derivative approximations are applied in the vicinity of the interface. To make the problem tractable, the conservation and interface movement equations were linearized. The details of these derivative approximations and linearizations will be given elsewhere[28].

REFERENCES

1. W.J. Cooper, P.D. Krasicky, and F. Rodriguez, Polymer, 26, 1069 (1985).
2. A.C. Ouano, in Polymers in Electronics, T. Davidson, ed., ACS Symposium Series 242, 1984, p. 79.
3. J.S. Greeneich, J. Electrochem. Soc., 122, 970 (1975).
4. J.H. Lai and L. Shepherd, J. Appl. Polym. Sci., 20, 2367 (1976).
5. E. Gipstein, A.C. Ouano, D.E. Johnson, and O.U. Need, Polym. Eng. Sci., 17, 396 (1977).
6. H.W. Deckman and J.H. Dunsmuir, J. Vac. Sci. Technol. B, 1, 1166 (1983).
7. N.L. Thomas and A.H. Windle, Polymer, 21, 613 (1980).
8. S. Matsuoka and T.K. Kwei, in Macromolecules: An Introduction to Polymer Science, F.A. Bovey and F.H. Winslow, eds., Academic Press, New York, 1979, p. 363.
9. L.F. Thompson and M.J. Bowden in Introduction to Microlithography, L.F. Thompson, C.G. Willson, and M.J. Bowden, eds., ACS Symposium Series 219, 1983, p. 161.
10. A.F.M. Barton, Handbook of Solubility Parameters and Other Cohesion Parameters, CRC Press, Inc., Boca Raton, Fl, 1983, p. 141.
11. D.W. van Krevelen, Properties of Polymers, Elsevier Scientific Publishing Co., Amsterdam, 1976, p. 141.
12. P.J. Flory, Principles of Polymer Chemistry, Cornell University Press, Ithaca, New York, 1953, p. 548.
13. J. Brandrup and E.H. Immergut, eds., Polymer Handbook, Wiley, New York, 1975, p. IV-131.
14. J.M. Prausnitz, Molecular Thermodynamics of Fluid-Phase Equilibria, Prentice-Hall, Englewood Cliffs, New Jersey, 1969, p. 297.
15. T.A. Alfrey, E.F. Gurnee, and W.G. Lloyd, J. Polym. Sci. (C), 12, 249 (1966).
16. F. Rodriguez, P.D. Krasicky, and R.J. Groele, Solid State Technol., 28(5), 125 (1985).
17. W.W. Flack, J.S. Papanu, D.W. Hess, D.S. Soong, and A.T. Bell, J. Electrochem. Soc., 131, 2200 (1984).
18. A. Zaghloul and R. Azzam, Surface Sci., 96, 169 (1980).
19. F.L. McCrackin, Natl. Bur. Std., Tech. Note 479 (1969).
20. B. Wu, MS Thesis, University of California, Berkeley, December 1982.
21. F. Asmussen and K. Ueberreiter, J. Polym. Sci., 57, 199 (1962).
22. Y. Tu and A.C. Ouano, IBM J. Res. Develop., 21, 131 (1977).
23. J.H. Petropoulos and P.P. Roussis, J. Memb. Sci., 3, 343 (1978).
24. J. Crank, J. Polym. Sci., 11, 151 (1953).
25. N.L. Thomas and A.H. Windle, Polymer, 21, 613 (1980).
26. C. Gostoli and G.C. Sarti, Polym. Eng. Sci., 22, 1018 (1982).
27. P.G. de Gennes and L. Leger, Ann. Rev. Phys. Chem., 33, 49 (1982).

28. J.S. Papanu, Ph.D. Dissertation, University of California, Berkeley, CA, 1987.
29. J. Crank, Free and Moving Boundary Problems, Clarendon Press, Oxford, 1984.

Table I. Sample Characteristics

M_n	$\frac{M_w}{M_n}$
27,000	1.11
46,400	2.01
66,700	1.08
89,100	1.10
163,000	1.10
180,000 *	2.8

All samples were obtained from Polysciences, Inc. except (*) which was obtained from KTI Chemicals, Inc.

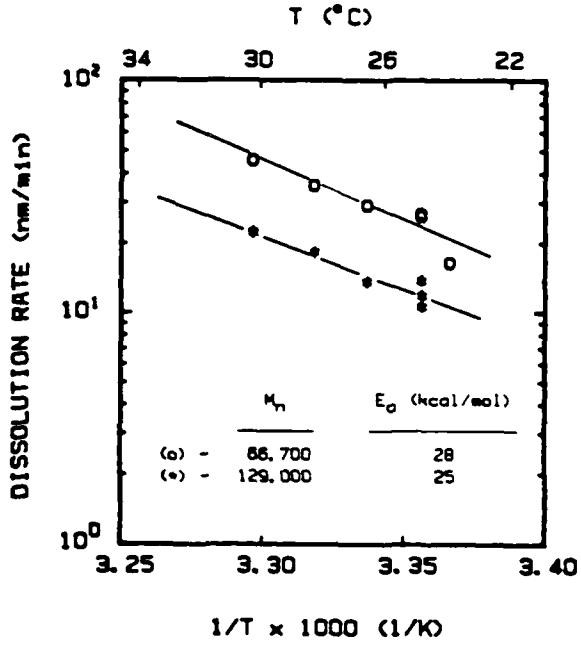

Figure 1. Arrhenius plot for the dissolution of ambient-quenched monodisperse (Mw/Mn <1.11) PMMA in MIBK.

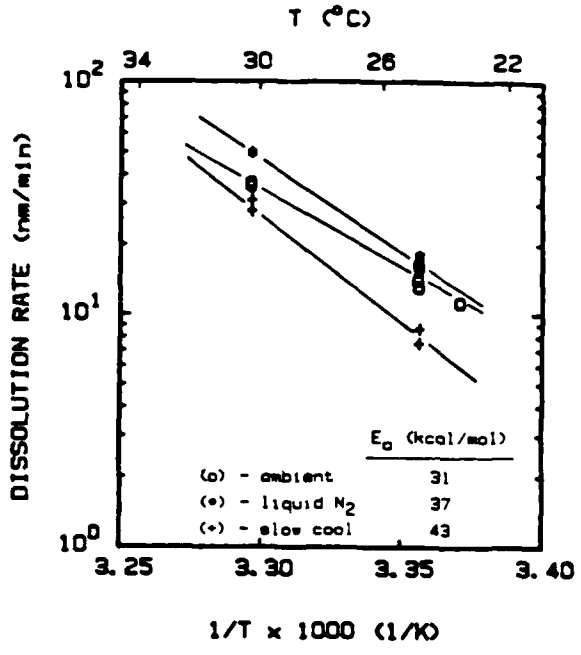

Figure 2. Arrhenius plot for the dissolution of polydisperse KTI PMMA resist for different softbake cooling rates.

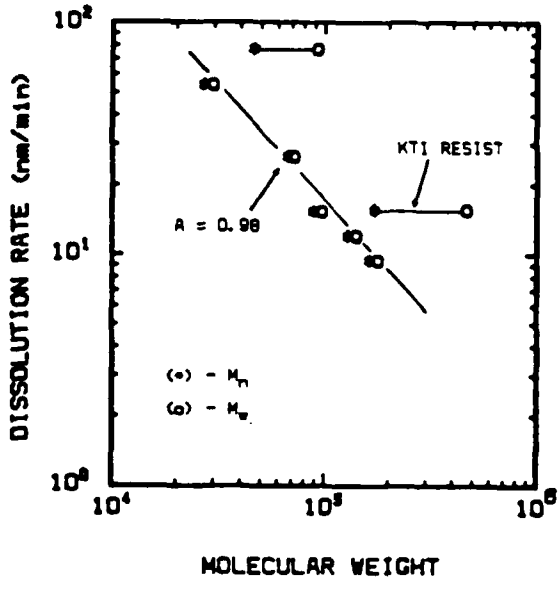

Figure 3. Effect of molecular weight and dispersity on the dissolution rate of ambient quenched PMMA in MIBK at 24.8°C.

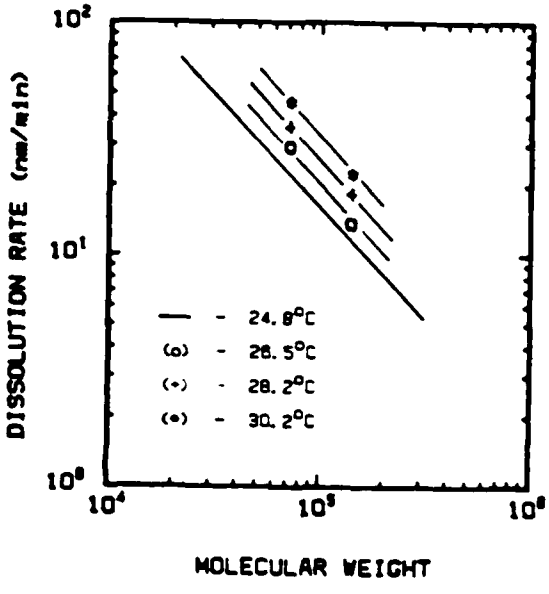

Figure 4. Dissolution rates of ambient quenched, monodisperse PMMA in MIBK at different temperatures.

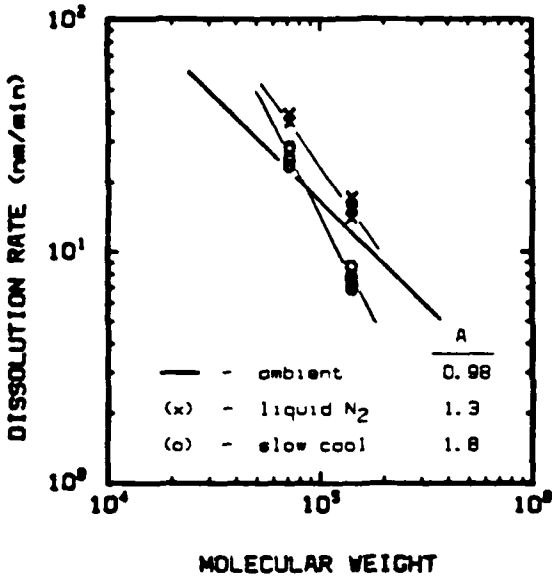

Figure 5. The effect of softbake cooling rate on the molecular weight exponent, A, for monodisperse PMMA in MIBK at 24.8°C.

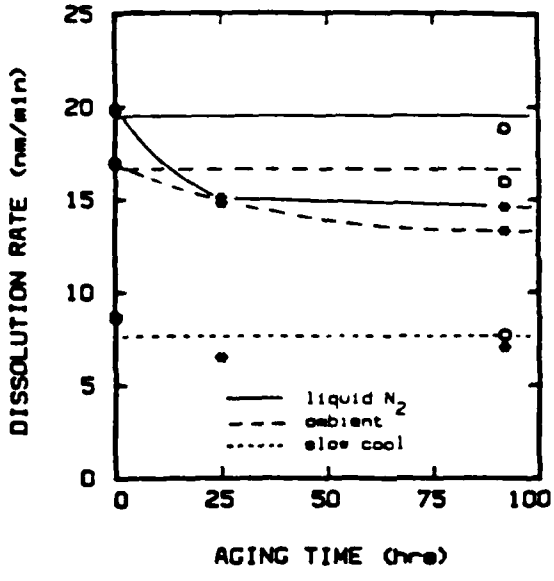

Figure 6. Aging effect on the dissolution rate of polydisperse KTI PMMA resist at 24.8°C for samples aged at room temperature (o) and at 60°C (•).

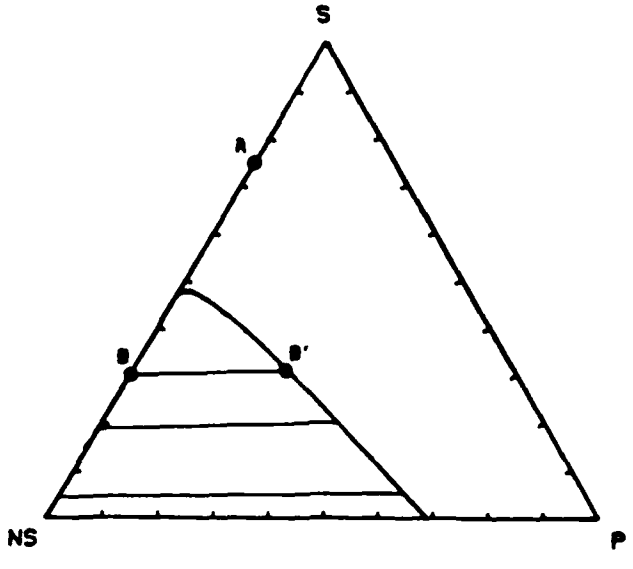

Figure 7. Ternary phase diagram for a nonsolvent(1), solvent(2), polymer(3) system taking $\chi_{23}=0$ and $\chi_{12}=\chi_{13}=1.0$; MW = 200,000.

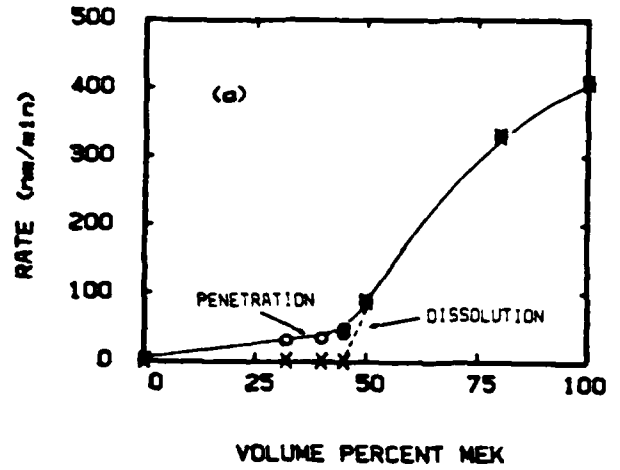

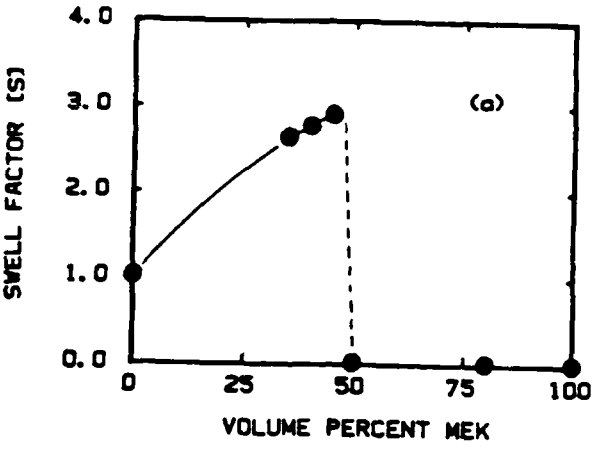

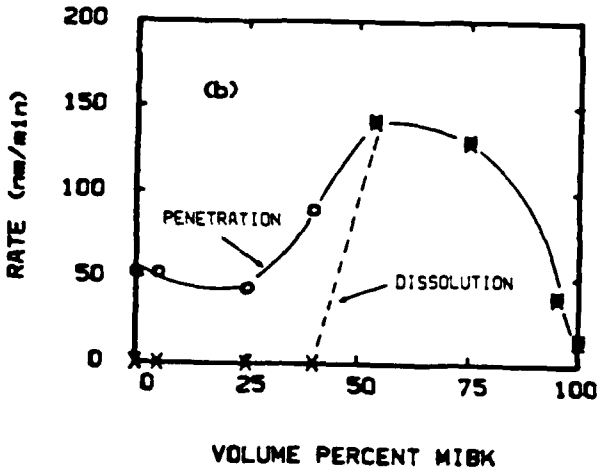

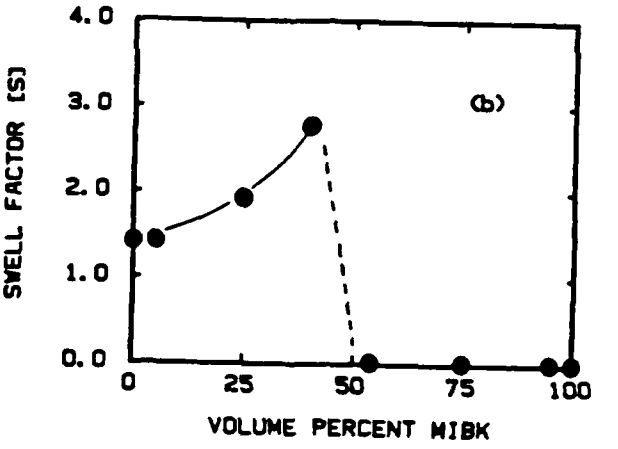

Figure 8. Penetration and dissolution rates of PMMA as function of solvent composition at 24.8°C for a) MEK/IpOH and b) MIBK/MeOH.

Figure 9. Swell factor (S) as a function of solvent composition at 24.8°C for a) MEK/IpOH and b) MIBK/MeOH. S is the ratio of the gel thickness at equilibium to the inital PMMA thickness (1.2 μm).

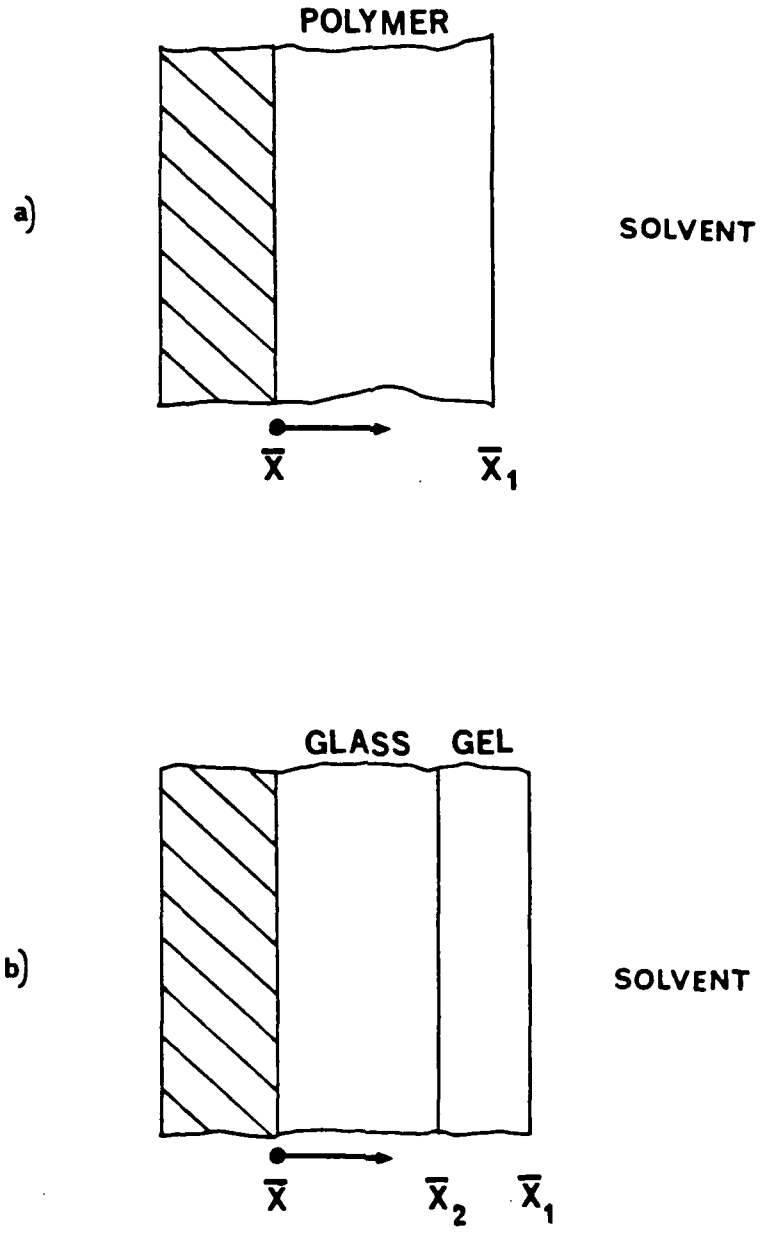

Figure 10. Coordinate system and interface positions for a) Fickian penetration and b) Case II penetration.

Appendix

Submitted to:
J. Electrochem. Soc.

Influence of Processing and Molecular Parameters on the Dissolution Rate of Poly-(Methyl Methacrylate) Thin Films

J. Manjkow, J.S. Papanu, D.W. Hess, D.S. Soong, and A.T. Bell
Department of Chemical Engineering
University of California
Berkeley, California 94720

ABSTRACT

The influence of processing and molecular parameters on the dissolution rate of poly-(methyl methacrylate), PMMA, thin films (<1 μm) in methyl isobutyl ketone, MIBK, was studied *in situ* with a single-element rotating-polarizer ellipsometer (psi-meter). Dissolution rates were highly sensitive to the molecular weight distribution, softbake cooling cycle and dissolution temperature. The apparent activation energy for the dissolution of PMMA in MIBK varied from 25 kcal/mol to 43 kcal/mol depending upon softbake cooling rates and molecular weight distribution. The dissolution rate of air quenched, monodisperse (M_w/M_n<1.11) PMMA samples was found to vary with the molecular weight to the -0.98 power. For slowly cooled samples this constant was 85% higher, suggesting improved contrast with slow cooling. Polydisperse samples (M_w/M_n≈2) dissolved about

twice as fast as monodisperse ones of the same number average molecular weight. Samples slowly cooled after softbaking and aged for 100 hours at room temperature or at 60°C showed no change in the dissolution rate with aging. However, the dissolution rate of samples cooled rapidly after softbaking and aged at 60°C decreased by as much as 25%.

INTRODUCTION

The dissolution of resist materials in a developer solution is a critical step in integrated circuit (IC) fabrication. Further, this step assumes greater importance as pattern size decreases and circuit density increases [1]. Nevertheless, few systematic studies on the effect of molecular weight distribution(MWD), softbake cooling rate, sample aging, and dissolution temperature on developed resist image have been reported.

The basis for lithographic image formation in IC fabrication is the relative dissolution rates of exposed and unexposed regions of the resist. For single-component resists, the dissolution rates in these regions differ because the molecular weight(MW) in the exposed regions has been altered by the radiation. With positive electron-beam resists, MW decreases upon exposure, thus enhancing solubility in the developer, whereas with negative resists MW increases, lowering solubility. The MW effect on PMMA dissolution has been investigated previously [2,3,4,5], but these studies have often shown dissimilar behavior for the dissolution rate dependence on MW. The effect of MWD on sensitivity and contrast has been reported [6,7,8], but no direct studies have been performed to compare dissolution rates of samples with different MWD's.

The effect of post-softbake cooling rate on resist dissolution is

often overlooked in IC fabrication processes. It has been reported [9] that the rate at which thick (1 mm) samples of PMMA were cooled through the glass transition temperature (T_g) affected the rate of methanol absorption. This effect is believed to be due to the 'freezing-in' of excessive free volume at higher cooling rates. The more free volume present in a polymer, the greater the penetration rate. Polymers are also known to undergo volume relaxation, whereby the trapped-in free volume decreases and approaches its equilibrium state with time [10,11]. This relaxation process can have important implications for resist dissolution, since the behavior of the resist may change as it ages.

In the present study, dissolution rates of PMMA in methyl isobutyl ketone, MIBK, were investigated <u>in situ</u> using a psi-meter [12,13]. To ascertain the effect of MW on the dissolution rate of PMMA, commercial MW standards of known dispersity, including several monodisperse samples, were used. All data presented in this paper are for unexposed PMMA. After softbaking, samples were cooled at different rates to determine the effect of cooling rate on film dissolution. Since aging allows volume relaxation in polymeric materials, samples prepared at different cooling rates were aged at room temperature($\approx$25^{o}C) and at 60^{o}C to determine the effect of post-cool aging on dissolution. Finally, apparent activation energies were obtained for different molecular weight dispersity and softbake cooling rates to determine how these factors affect the temperature sensitivity of dissolution.

EXPERIMENTAL

Materials

Commercial PMMA standards of known MWD were obtained from Polysciences, Inc. Sample characteristics (M_n and M_w/M_n) are shown in Table 1. PMMA standards were dissolved in chlorobenzene to a concentration of approximately 8 volume percent. In addition, a polydisperse (M_n=180,000; M_w/M_n=2.8) PMMA electron-beam resist (6 weight percent in chlorobenzene) was obtained from KTI Chemicals, Inc. The molecular weight distribution of the KTI resist was determined by gel permeation chromatography [14].

Procedures

The PMMA solutions were spin-coated onto silicon wafers at approximately 2000 RPM. Samples were softbaked at 160°C for one hour in a nitrogen purged, convection oven and then either cooled gradually inside the oven or quenched in either liquid nitrogen or in ambient. The cooling rate through T_g for the slowly cooled samples was approximated as 0.8°C/min by monitoring the oven temperature. Thickness measurements of

these softbaked films were made with a Sloan Dektak Profilometer and confirmed with an Applied Materials AME-500 Manual Ellipsometer. The average thickness was 0.65 μm.

For aging studies, one wafer for each of the cooling rates was broken into approximately 2 cm^2 pieces. Half of these pieces were placed inside a nitrogen purged, light filtered glove box at room temperature; the other half inside a nitrogen purged, convection oven maintained at 60°C. Dissolution took place in an optical cell [15] through which MIBK was circulated at about 25 ml/min. The cell temperature was controlled to within $\pm$0.1°C with a Yellow Springs Instrument Co., Inc, Model 72 Proportional Temperature Controller.

Rate Measurement

In our studies, a modified version [15] of the psi-meter described earlier [12] was used for <u>in situ</u> monitoring of dissolution. A psi-meter is a single-element rotating-polarizer ellipsometer in which an incident laser beam is polarization modulated and the intensity fluctuation of the reflected light measured. The ratio of the AC and DC components of the reflected intensity is related to the optical parameter psi (ψ) by AC/DC=-cos2ψ [13]. To determine film thickness as a function of time, calculated values of ψ or AC/DC are compared to experimental data. This was produced using an ellipsometry program [16] which gives theoretical values of ψ versus thickness when the wavelength, angle of incidence, and

refractive indices of the substrate, film, and immersion medium are known. For this study, the angle of incidence was 75^{o} and the wavelength was 632.8 nm. Values of ψ (or equivalently AC/DC) were collected continuously during dissolution at a rate of one point per second so that film thickness variation could be followed easily.

RESULTS AND DISCUSSION

Figure 1a shows the AC/DC signal as a function of time for a typical dissolution run. Figure 1b shows calculated AC/DC versus film thickness for PMMA on a silicon substrate immersed in MIBK. Since the initial thickness is measured prior to a run, the starting point is known, and the time-dependent thickness can be followed. The oscillatory time dependence of AC/DC is indicative of a constant dissolution rate with minimal surface swelling. This linear time dependence, common for glassy polymers, results from a relaxation controlled process known as Case II transport [9,17].

In order to rationalize the linear behavior, both steps of the dissolution process must be considered. First, solvent must penetrate the glassy polymer matrix which results in local swelling and converts the glass into a swollen gel. Then the polymer chains, which are more mobile due to the presence of solvent, disentangle from the surface of the swollen polymer and diffuse into the bulk solvent. If the penetration occurs by Case II transport, and disentanglement is rapid relative to penetration, then a constant dissolution rate with limited surface swelling is expected.

A constant dissolution rate was observed for all PMMA/MIBK dissolution experiments discussed in this paper. A forthcoming companion article will address the effects of solvent/nonsolvent composition on

PMMA film dissolution [18].

Temperature Effect

Dissolution of polymers is often viewed as an activated process following an Arrhenius-type rate expression [5,19]:

$$R_d = k \exp(-E_a/RT) \qquad (1)$$

where: R_d = dissolution rate
E_a = effective activation energy
T = absolute temperature
R = gas constant
k = constant

Often, no single activation energy can adequately describe the dissolution process; thus, deviations from the behavior predicted by Eqn 1 have been observed [20]. If these deviations are not large, Eqn 1 is applicable over a moderate temperature range. Further, when the temperature range selected corresponds to typical operating temperatures used in IC development processes, then Eqn 1 can be useful for predictive purposes.

Figure 2 shows the effect of temperature on the dissolution of air quenched, monodisperse (M_w/M_n<1.11) PMMA. The apparent activation energies are nearly the same for the two molecular weights, indicating

that E_a is not a strong function of molecular weight for monodisperse PMMA. The average value of 27 kcal/mol is in good agreement with the value of 24 kcal/mol obtained previously [5]. These relatively high activation energies are indicative of Case II penetration [9].

The effect of temperature on the dissolution of polydisperse KTI PMMA resist for different softbake cooling rates is presented in Figure 3. The rather high E_a of 43 kcal/mol for the slowly cooled KTI PMMA resist indicates strong temperature sensitivity for the dissolution process. A change in dissolution temperature of only 1°C in the vicinity of 25°C can affect the dissolution rate by over 25%. The E_a of a slowly cooled KTI resist is 40% greater than that of an air quenched KTI resist and nearly 60% greater than that of an air quenched, monodisperse sample (Fig 2). This wide range in apparent activation energies due to different cooling rates demonstrates the importance of sample handling after softbaking. A correlation exists between the rate at which a resist is cooled and its subsequent dissolution rate. At a given temperature, the dissolution rate is highest for the sample having undergone the fastest cooling rate (i.e. liquid nitrogen quench) and lowest for the slowest cooling rate.

Molecular Weight Effect

The dissolution rates of polystyrene in a number of solvents were found to vary with molecular weight according to the following expression [21]:

$$R_d = k\, M^{-A} \qquad (2)$$

where: R_d = dissolution rate
M = molecular weight
A,k = constants

This relation was found to hold for molecular weights between 1000 and 350,000. Below this range, the dissolution rate was slightly greater than predicted by Eqn 2. Above a molecular weight of 350,000, the dissolution rate dropped off sharply. This effect was thought to be caused by the greater chain entanglement at higher molecular weights.

The observed dissolution rates are plotted as a function of the number and weight average molecular weights of mono- and polydisperse PMMA in Figure 4. (See Table 1 for values of M_n and M_w/M_n). For monodisperse samples, a linear dependence exists in this log-log plot of dissolution rate versus MW, consistent with the behavior predicted by Eqn 2. The value of the MW exponent, A, was found to be 0.98. Previous

authors [2,5] have observed a non-linear log-log dependence on MW, since a larger MW range was studied than in this work.

It can also be seen from Figure 4 that at a given M_n or M_w, the dissolution rate of a polydisperse sample is higher than that of a monodisperse sample. This effect is believed to be due to the wider MWD of polydisperse samples. Shorter chains dissolve at a faster rate than longer chains according to Eqn 2 and, after their removal, allow facile penetration of the polymer by solvent which improves the mobility of the longer chains. This effect enhances the overall dissolution rate of the polydisperse polymer relative to a monodisperse polymer of the same M_n.

The dissolution of air quenched, monodisperse PMMA was carried out at several temperatures and the results are presented in Figure 5. It can be seen that A is independent of temperature. This effect has been observed previously [5,21].

Figure 6 shows the effect of cooling rate on A for monodisperse PMMA samples. If a resist sample is slow cooled, instead of air quenched, A can be increased to 1.8. It is desirable to have A as large as possible in order to obtain high contrast lithography [5]. This higher contrast is due to a greater difference in solubility rate between exposed and unexposed regions of the resist for larger A (Eqn 2). Thus, slowly cooling a resist after softbaking may enhance the contrast. While this conclusion is based on data for a limited molecular weight range, it suggests greater attention be given to the softbake cooling rate.

Aging Effect

Figure 7 shows the aging effect on the dissolution of polydisperse KTI resist for different cooling rates. Samples were aged at room temperature or at 60°C as indicated. There was no apparent change in the dissolution rate for samples aged at room temperature over a period of 100 hours. Also, samples that were cooled slowly after softbaking showed no significant change in the dissolution rate for the same aging period. However, the liquid nitrogen and air quenched samples which were aged at 60°C showed a noticeable decrease in the dissolution rate after the first 24 hours and a gradual decrease thereafter. These observations can be explained in terms of changes in the free volume of the polymer.

The rate at which a polymer is cooled through T_g will determine the amount of free volume 'frozen-in'; the greater the rate, the greater the free volume. In time, the polymer chains relax and the free volume fraction decreases toward its equilibrium state of 0.025 [10,11]. For samples cooled gradually after softbaking, it appears the polymer has adequate time to closely establish its equilibrium free volume, and relaxation, if any, occurs extremely slowly and insignificantly as to evade detection. Hence, aging these samples at room temperature or at 60°C exerts a negligible effect on their dissolution rate.

Unlike the slowly cooled samples, the liquid nitrogen and air quenched samples displayed a relaxation effect due to aging at 60°C (Fig 7) With sufficient time, these quenched samples would be expected to approach the equilibrium free volume and, hence, dissolve at a comparable rate to slowly cooled ones. The samples aged at room temperature show no change in dissolution rate, but the relaxation rate is probably so slow that the effect on dissolution is negligible. With sufficient aging, these samples would also be expected to show a decrease in dissolution rate.

CONCLUSIONS

In order to gain a fundamental understanding of the kinetics of resist dissolution, it is imperative that each processing step leading to the ultimate development be scrutinized. Previously, the effect of softbake cooling rate, the high temperature sensitivity of the dissolution process and, to some extent, the effect of molecular weight dispersity were often ignored. Our study has shown that these parameters dramatically affect the dissolution process.

The effect of cooling rate was found to be of particular importance since E_a and the molecular weight exponent, A, were found to vary by as much 85% depending on the cooling rate. In particular, A was 0.98 for air quenched and 1.8 for slowly cooled monodisperse polymer samples. PMMA of broad MWD's was found to dissolve at a faster rate than monodisperse samples of the same M_n. For air quenched, monodisperse samples, the dissolution rate was found to vary with the molecular weight to the -0.98 power. At relatively low temperatures and for short periods of time, the effect of aging on PMMA appears to be minimal. However, for samples annealed at elevated temperatures or samples aged for a long time, the aging effect becomes significant.

Acknowledgment

This project was supported by the Air Force Office of Scientific Research under Grant AFOSR-90-0078.

REFERENCES

1. D.J. Elliot, Integrated Circuit Fabrication Technology, McGraw-Hill Book Company, New York, 1982, p. 209.

2. W.J. Cooper, P.D. Krasicky, and F. Rodriguez, Polymer, 26, 1069 (1985).

3. A.C. Ouano, in Polymers in Electronics, T. Davidson, ed., ACS Symposium Series 242, American Chemical Society, Washington, D.C., 1984, p. 79.

4. J.S. Greeneich, J. Electrochem. Soc., 121, 1669 (1974).

5. J.S. Greeneich, J. Electrochem. Soc., 122, 970 (1975).

6. J.H. Lai and L. Shepherd, J. Appl. Polym. Sci., 20, 2367 (1976).

7. E. Gipstein, A.C. Ouano, D.E. Johnson, and O.U. Need, Polym. Eng. Sci., 17, 396 (1977).

8. H.W. Deckman and J.H. Dunsmuir, J. Vac. Sci. Technol. B, 1, 1166 (1983).

9. N.L. Thomas and A.H. Windle, Polymer, 21, 613 (1980).

10. F.W. Billmeyer, Textbook of Polymer Science, Wiley-Interscience, New York, 1984, p. 59.

11. S. Matsuoka and T.K. Kwei, in Macromolecules: An Introduction to Polymer Science, F.A. Bovey and F.H. Winslow, eds., Academic Press, New York, 1979, p. 363.

12. W.W. Flack, J.S. Papanu, D.W. Hess, D.S. Soong, and A.T. Bell, J. Electrochem. Soc., 131, 2200 (1984).

13. A. Zaghloul and R. Azzam, Surface Sci., 96, 169 (1980).

14. B. Wu, MS Thesis, University of California, Berkeley, December 1982.

15. J. Manjkow, MS Thesis, University of California, Berkeley, December 1986.

16. F.L. McCrackin, Natl. Bur. Std., Tech. Note 479 (1969).

17. T.A. Alfrey, E.F. Gurnee, and W.G. Lloyd, J. Polym. Sci. (C), 12, 249 (1966).

18. J. Manjkow, J.S. Papanu, D.S. Soong, D.W. Hess, and A.T. Bell, to be published.

19. G.S. Park, in Characterization of Coatings: Physical Techniques, R.R. Raymond and J.S. Long, eds., Treatise on Coatings Vol. 2, 1976, p. 488.

20. N. Thomas and A.H. Windle, Polymer, 19 255 (1978).

21. F. Asmussen and K. Ueberreiter, J. Polym. Sci., 57, 199 (1962).

Table I. Sample Characteristics

M_n	$\frac{M_w}{M_n}$
27,000	1.11
46,400	2.01
66,700	1.08
89,100	1.10
163,000	1.10
180,000 *	2.8

All samples were obtained from Polysciences, Inc. except (*) which was obtained from KTI Chemicals, Inc.

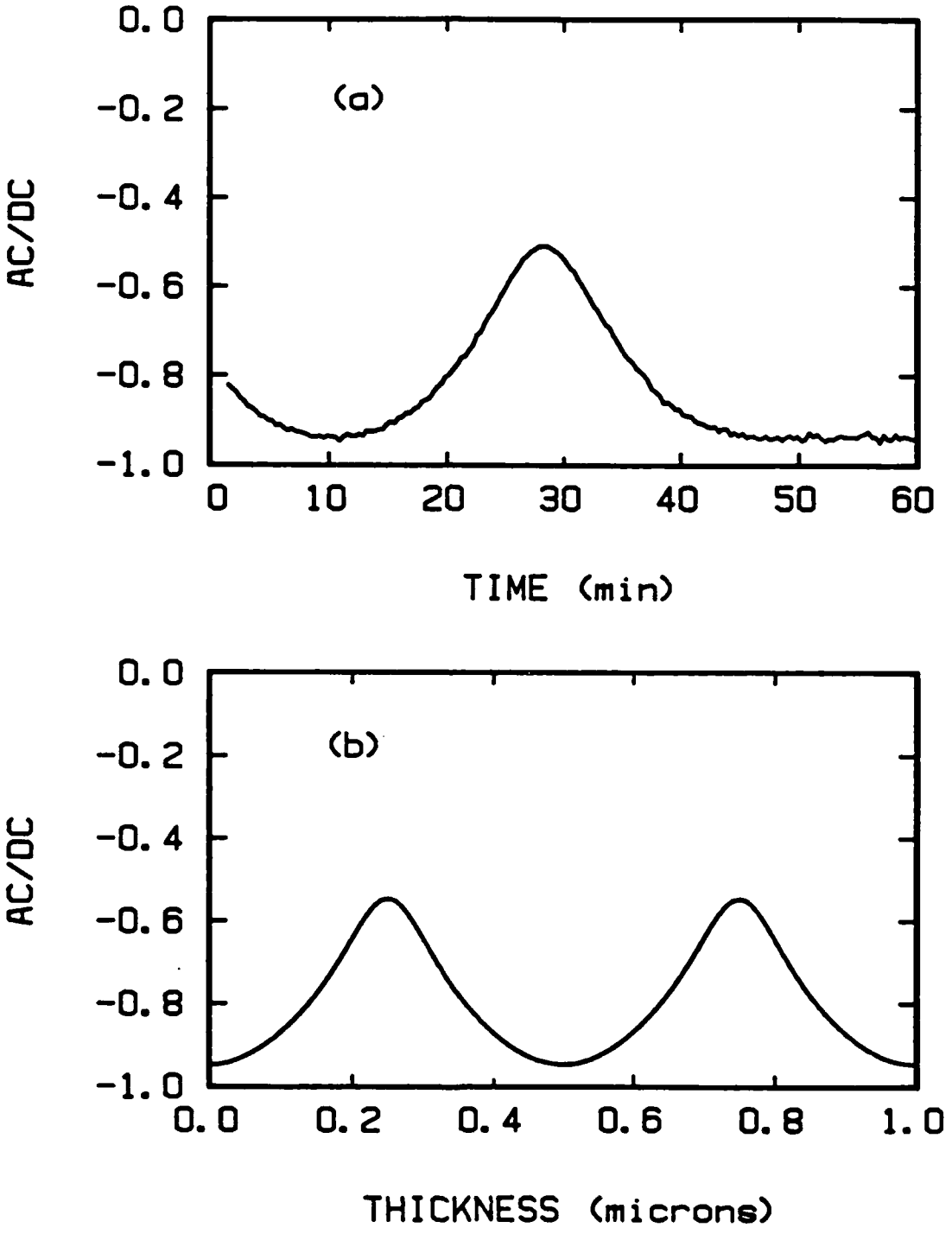
0.0
-0.2
-0.4
-0.6
-0.8
-1.0
AC/DC
(a)
0
10
20
30
40
50
60
TIME (min)
0.0
-0.2
-0.4
-0.6
-0.8
-1.0
AC/DC
(b)
0.0
0.2
0.4
0.6
0.8
1.0
THICKNESS (microns)

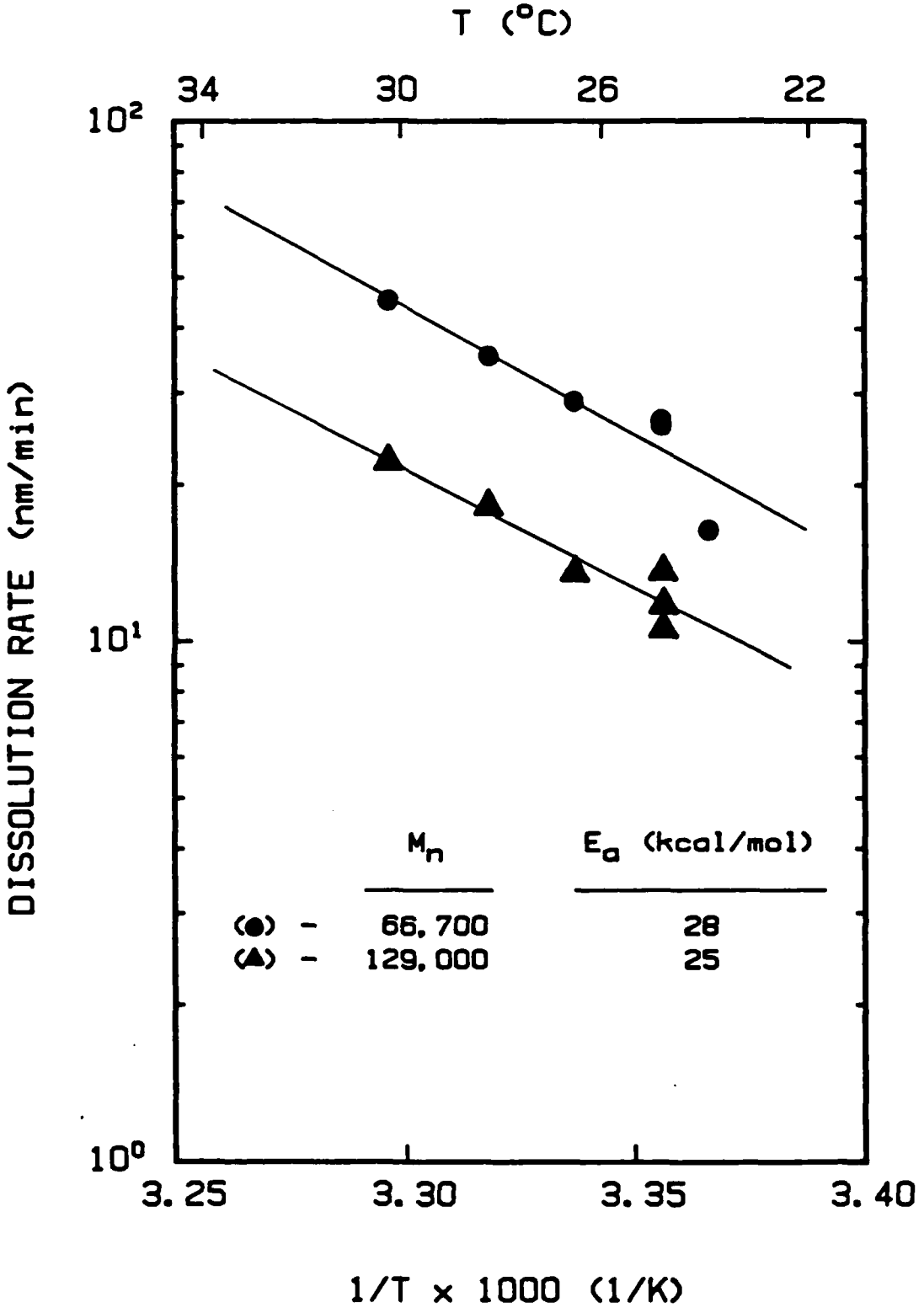
T (°C)
34
30
26
22
10^2
10^1
10^0
DISSOLUTION RATE (nm/min)
M_n
E_a (kcal/mol)
(●) – 66,700 28
(▲) – 129,000 25
3.25
3.30
3.35
3.40
1/T x 1000 (1/K)

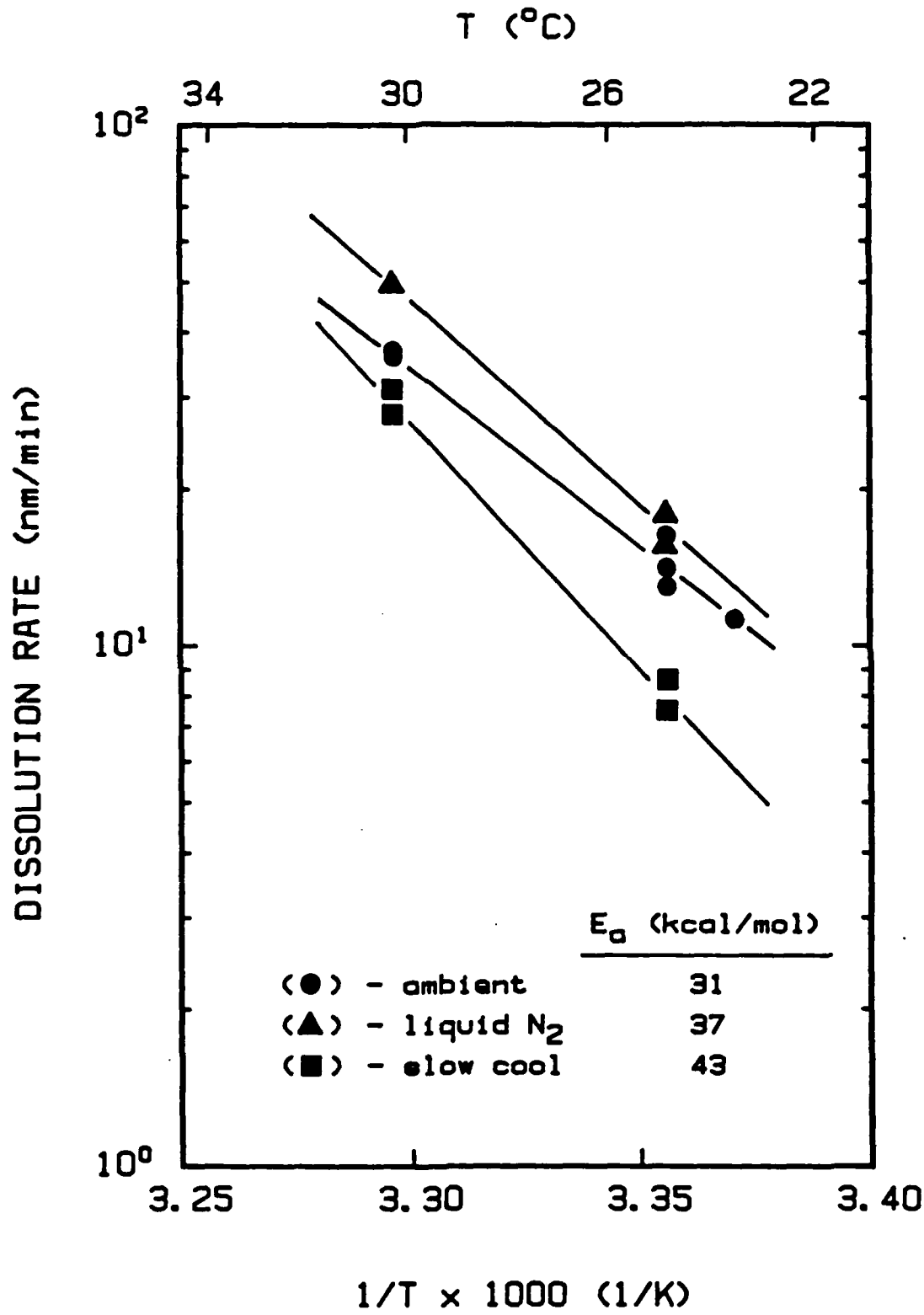
T (°C)
34
30
26
22
10^2
10^1
10^0
DISSOLUTION RATE (nm/min)
3.25
3.30
3.35
3.40
1/T x 1000 (1/K)
E_a (kcal/mol)
(●) - ambient 31
(▲) - liquid N_2 37
(■) - slow cool 43

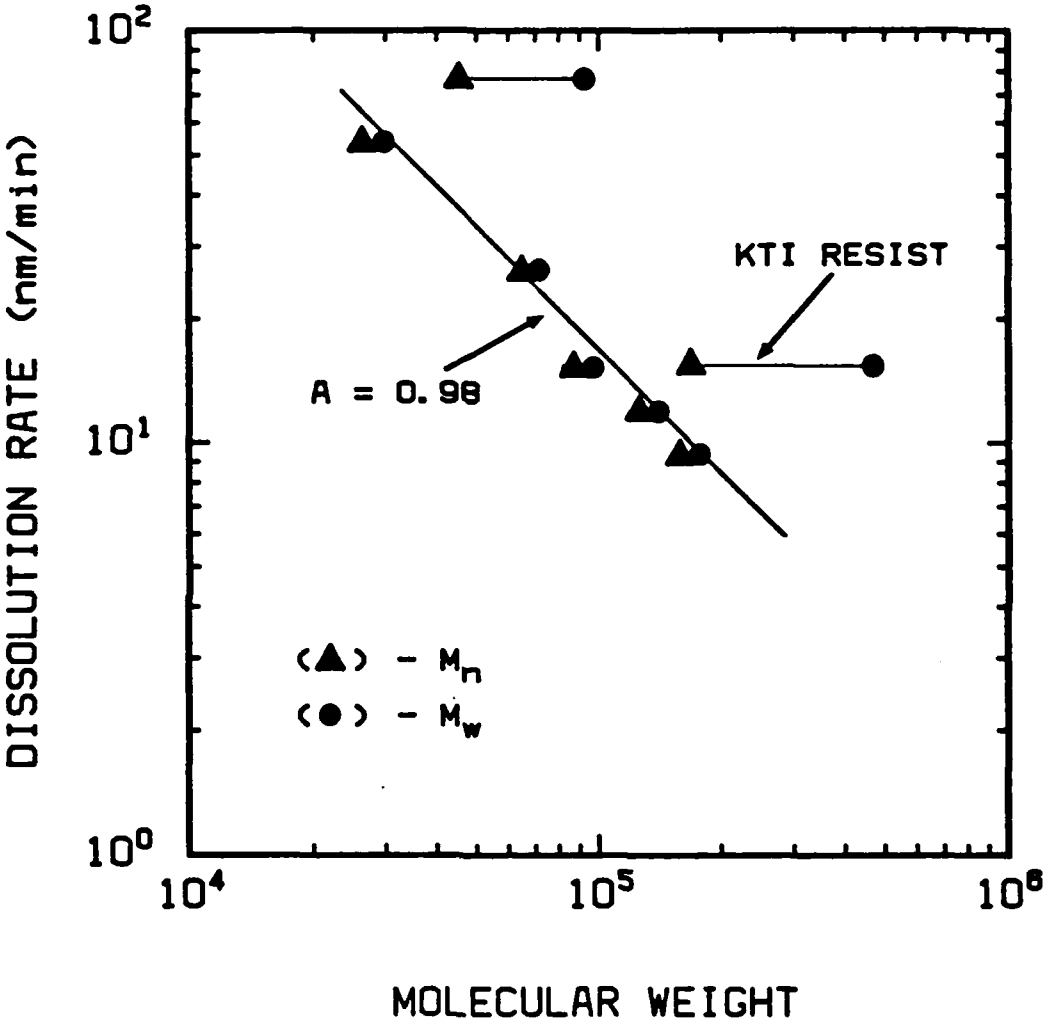
10^2
10^1
10^0
DISSOLUTION RATE (nm/min)
KTI RESIST
A = 0.98
(▲) - M_n
(●) - M_w
10^4
10^5
10^6
MOLECULAR WEIGHT

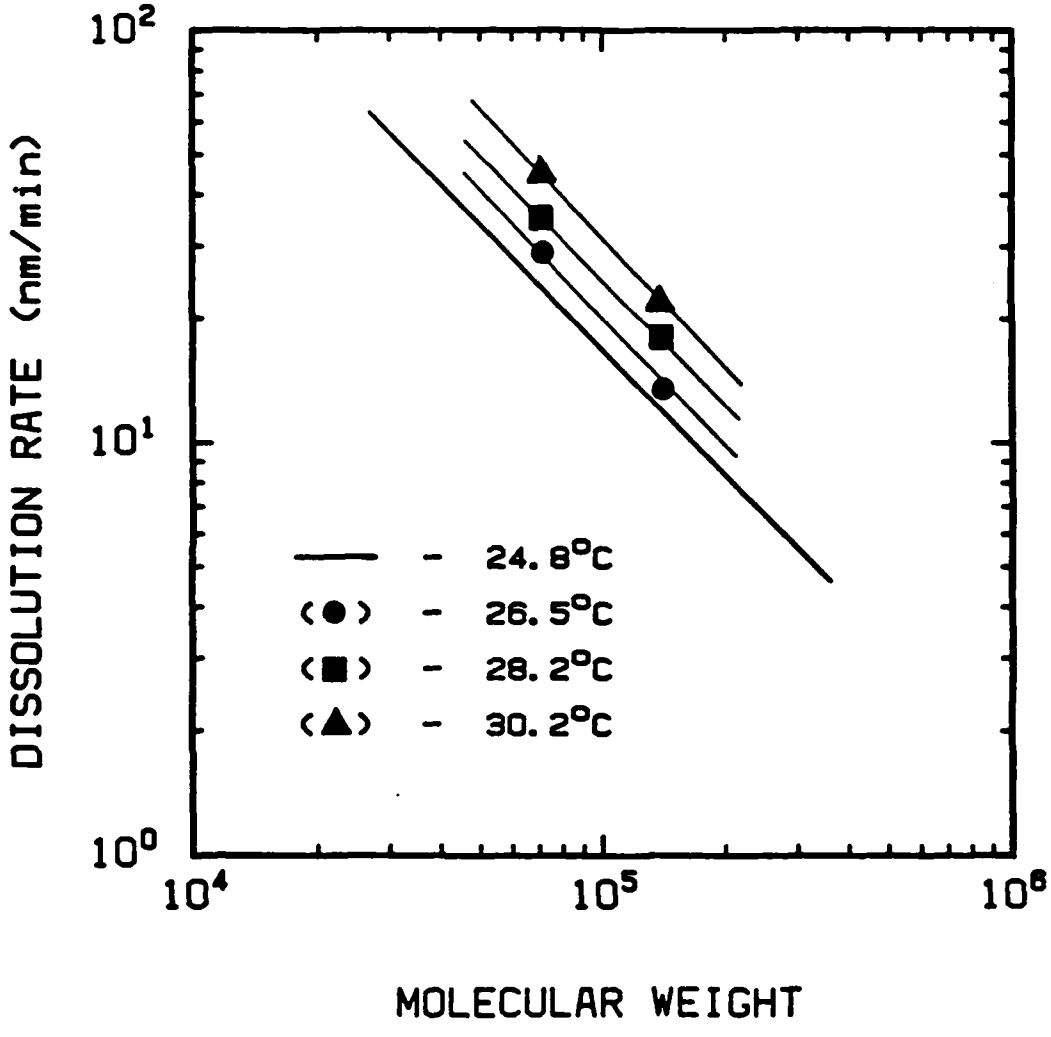
DISSOLUTION RATE (nm/min)
10^2
10^1
10^0
10^4
10^5
10^6
MOLECULAR WEIGHT
— - 24.8°C
(●) - 26.5°C
(■) - 28.2°C
(▲) - 30.2°C

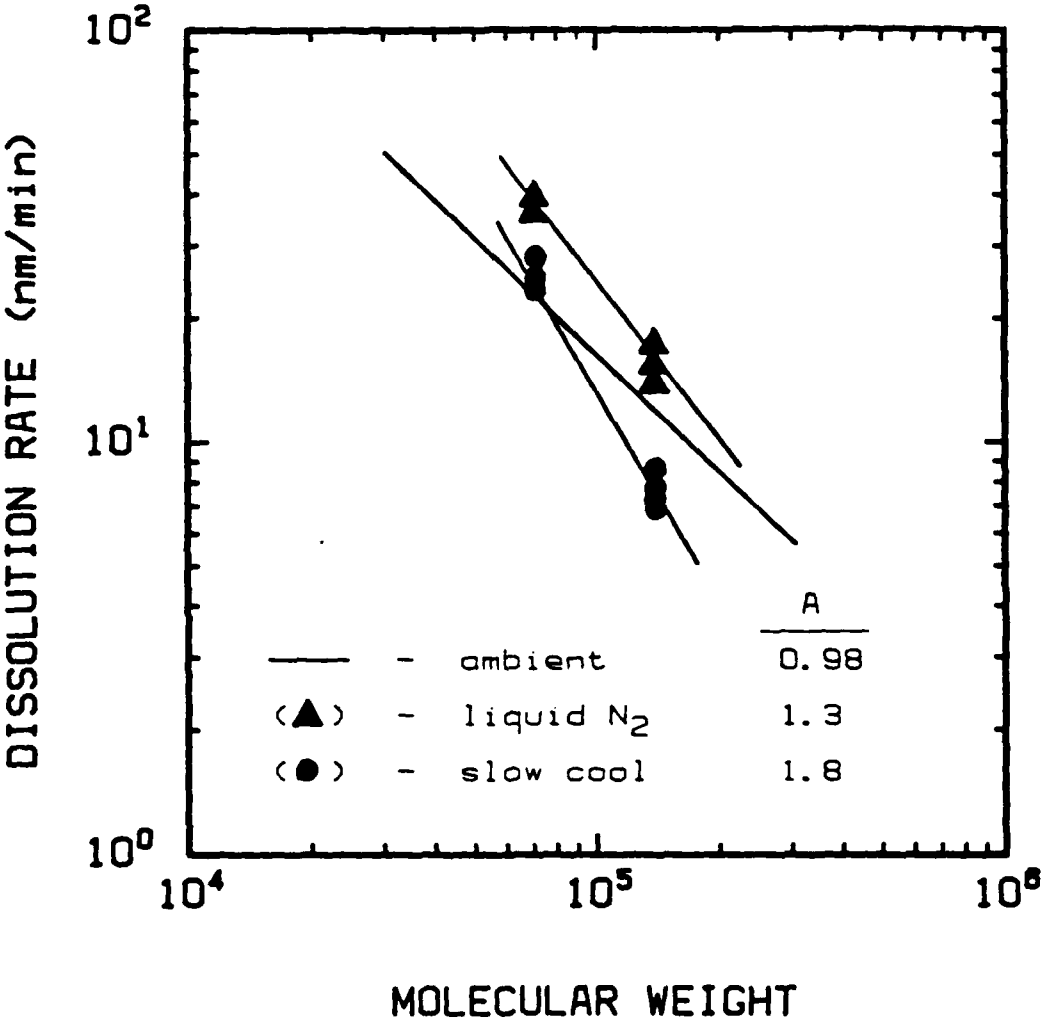
DISSOLUTION RATE (nm/min)
10^2
10^1
10^0
10^4
10^5
10^6
MOLECULAR WEIGHT
A
— - ambient 0.98
(▲) - liquid N_2 1.3
(●) - slow cool 1.8

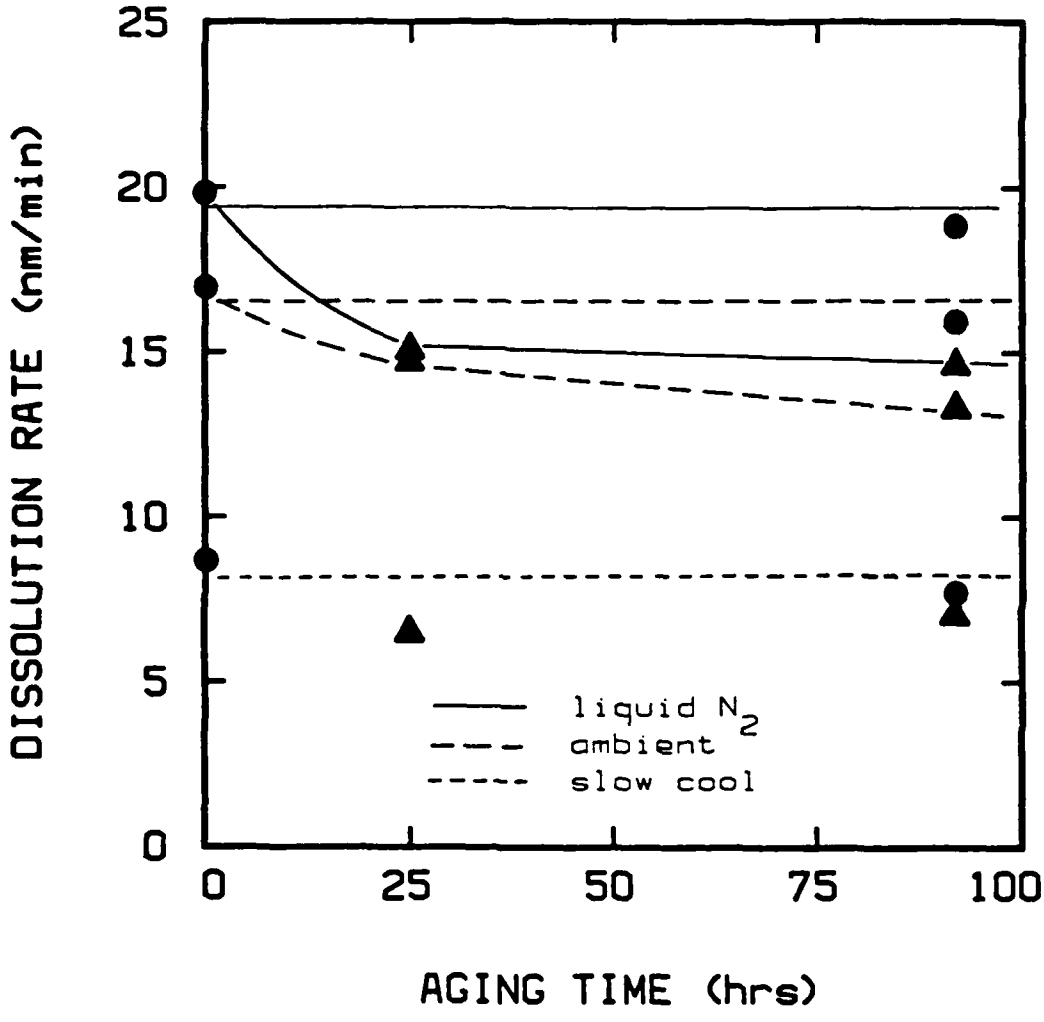
DISSOLUTION RATE (nm/min)
25
20
15
10
5
0
0
25
50
75
100
AGING TIME (hrs)
liquid N_2
ambient
slow cool

submitted to:
J. Appl. Phys.

An *In Situ* Study of Dissolution and Swelling Behavior of Poly-(Methyl Methacrylate) Thin Films in Solvent/Nonsolvent Binary Mixtures

J. Manjkow, J.S. Papanu, D.S. Soong, D.W. Hess, and A.T. Bell
Department of Chemical Engineering
University of California
Berkeley, California 94720

ABSTRACT

A single-element rotating-polarizer ellipsometer (psi-meter) was used for *in situ* characterization of the thermodynamic and kinetic behavior of poly-(methyl methacrylate), PMMA, thin films (1.2μm) in solvent/nonsolvent binary mixtures of methyl ethyl ketone/isopropanol (MEK/IPA) and methyl isobutyl ketone/methanol (MIBK/MeOH). Thermodynamic effects were inferred from equilibrium behavior by the degree of swelling and polymer-solvent solubility. A sharp transition between complete solubility and almost total insolubility was observed in a narrow concentration range near 50:50 (by volume) solvent/nonsolvent for both MEK/IPA and MIBK/MeOH. In the insoluble regime, the polymer was found to swell up to three times the initial thickness. At 50:50 MEK/IPA, a temperature decrease from 24.8°C to 18.4°C caused a change from complete dissolution to combined

swelling/dissolution behavior and rendered the PMMA film only 68% soluble. Kinetic effects were determined by dissolution and penetration rate measurements. A constant penetration velocity was observed for almost all compositions for both binary solvent mixtures with Case II transport assumptions providing good agreement with experimental results. For MEK/IPA, penetration rates increased with increasing MEK concentration. For MIBK/MeOH, however, a maximum was observed at 60:40 MIBK/MeOH.

INTRODUCTION

In the fabrication of integrated circuits (IC's), development of exposed resists often involves the use binary solvent mixtures which typically consist of a strong solvent and a moderating nonsolvent [1]. The effects these solvent/nonsolvent developers exert on the swelling and dissolution behavior of resists are complex and their interpretation has generally been accomplished by noting the topographical profiles of the device. Distorted geometries often arose due to excessive swelling during dissolution. Clearly, as IC pattern sizes decrease and circuit density increases, swelling effects may become an important resolution controlling factor. The ability to systematically monitor, *in situ*, simultaneous dissolution and swelling of resists in solvent mixtures can provide insight into the complex mechanisms of resist development processes.

During a development process, solvent penetration and resist dissolution are controlled by kinetic and thermodynamic solvent/polymer interactions. In general, solvent mobility is primarily related to its molecular size whereas thermodynamic compatibility is associated with the strength of the interactions between structural groups of both polymer and solvent molecules [2].

An approximate measure of thermodynamic compatibility is given by the solubility parameter, δ [3]. Complete polymer-solvent miscibility

occurs when the δ's of polymer and solvent do not differ by more than 4.00 MPa for systems in which nonpolar forces are the dominant interaction [4]. A 'three-dimensional' solubility parameter model that accounts for hydrogen bonding and polar interactions as well has also been described [5,6].

Another measure of polymer-solvent compatibility is given by the Flory-Huggins interaction parameter, χ_{ij}, where the subscripts refer to pair interactions in multi-component systems [7]. Typically, complete polymer-solvent miscibility is expected for $\chi_{ij}<0.5$ [8]. Values of χ_{ij} for some polymer-solvent systems can either be found in the literature [9] or roughly calculated from solubility parameters [5,8]. Unfortunately, tabulated values for polymer solubility parameters can range widely [10] and data for χ_{ij} are somewhat limited [9].

Solvent or nonsolvent diffusion in glassy polymers is often characterized by a constant penetration velocity [11,12]. This non-Fickian behavior, termed Case II diffusion [13], is controlled by polymer relaxation and is characterized by a front of constant penetrant composition that invades the glassy polymer at a constant rate. For nonsolvent penetration, concentration in the solvent swollen gel layer remains constant and the mass uptake is linear with time [11,14]. In the case of strong solvents, the gel layer rapidly dissolves into the solvent and its thickness is typically not detectable. Thus with strong solvents, Case II diffusion gives rise to a constant dissolution rate [12].

These two limiting cases of total gel conversion in nonsolvent mixtures and 'immeasurable' gel formation in strong solvents are presented to illustrate the extremes in expected behavior. At intermediate conditions, it is conceivable that significant gel formation could occur in conjunction with polymer dissolution.

In this paper, effects of solvent-nonsolvent composition on the thermodynamic and kinetic behavior of poly-(methyl methacrylate), PMMA, thin films (1.2μm) will be examined *in situ* using a single-element rotating-polarizer ellipsometer (psi-meter). Thermodynamics will be expressed in terms of polymer solubility while kinetics will be represented as solvent penetration rates. A preliminary interpretation of data displaying simultaneous swelling and dissolution behavior will be given.

EXPERIMENTAL

Materials

A commercial PMMA electron-beam resist (6 weight percent in chlorobenzene) was obtained from KTI Chemicals, Inc. The heterogeneity index (M_w/M_n) of the resist was determined by gel permeation chromatography to be 2.8 with a number average molecular weight, M_n, of 180,000 [15]. The binary solvent mixtures were methyl ethyl ketone/isopropanol (MEK/IPA) and methyl isobutyl ketone/methanol (MIBK/MeOH). Based on solubility parameter data [16,17], MEK and MIBK are solvents for PMMA, whereas the alcohols are nonsolvents.

Procedures

The resist solution was spin-coated onto silicon wafers at approximately 1500 RPM. The samples were softbaked at 160°C for one hour in a nitrogen purged, convection oven and then quenched in ambient. Thickness measurements were made with a Sloan Dektak Profilometer and confirmed with an Applied Materials AME-500 manual ellipsometer. The average thickness of these softbaked films was 1.2 μm. Solutions of MEK/IPA or MIBK/MeOH were circulated through an optical cell [18] at about 25 ml/min. This gave an inlet velocity of 80 cm/min and an average channel velocity of 5.2 cm/min based on the inlet tubing and cell cross sectional areas, respectively. Above 25 ml/min, turbulence resulted which caused significant fluctuations in the optical signal. Reducing

the flow rate below 25 ml/min did not alter the dissolution rates, suggesting external mass transfer limitations to be relatively unimportant under such operating conditions. The cell temperature was maintained to $\pm 0.1^{\circ}C$ with a Yellow Springs Instrument Co., Inc, Model 72 Proportional Temperature Controller.

Rate Measurement

In our studies, a modified version [18] of the psi-meter described earlier [19,20] was used for *in situ* monitoring of dissolution and swelling rates. A psi-meter is a single-element rotating-polarizer ellipsometer which modulates the polarization of an incident laser beam and measures the intensity fluctuation of the reflected light. The ratio of the AC to DC component of the reflected intensity is related to the optical parameter, ψ, by $AC/DC = -\cos 2\psi$ [21]. For these experiments, a 2 mW He-Ne laser (wavelength 632.8 nm) was used. The angle of incidence was 75°. Values of AC/DC were collected continuously at a rate of one point per second.

Various diffusion models were incorporated into a modified ellipsometry program [22] to produce theoretical values of AC/DC versus time, which were then compared to experimental results. This program required the physical parameters of the psi-meter and polymer-solvent-nonsolvent system such as wavelength, angle of incidence, and refractive indices of the substrate, film, and immersion medium. An Abbe refractometer was used to correlate the mixture refractive index with the composition of MEK/IPA or MIBK/MeOH binary developer.

RESULTS AND DISCUSSION

MEK/IPA - Composition Effect

Figure 1a is an AC/DC trace for a 1.2 μm PMMA film immersed in 40:60 MEK/IPA at 24.8^{o}C. Thickness measurements at the completion of the run indicated that less than 2% of the PMMA dissolved at these conditions. Hence, the change in AC/DC signal in Figure 1a is due primarily to swelling effects, i.e. solvent penetration with very little polymer dissolution. For a Case II transport model, the penetration velocity is simply the ratio of the initial thickness of the glassy polymer to the total time of penetration. Determination of the gel layer composition during penetration is not as straightforward. To do so, a gel layer composition must be assumed and the resulting predicted AC/DC behavior compared to experimental results. Consistent with Case II diffusion, the composition profile in the gel layer is assumed flat.

Figure 1b shows a predicted plot of AC/DC versus time for Case II penetration assuming no polymer dissolves, a gel layer composition of 36% PMMA and a penetration velocity of 43.5 nm/min. Also shown in Figure 1b are the relative positions of the solvent/gel and gel/glass interfaces at various times during the swelling process assuming the volumes of polymer and solvent are ideally additive. Since virtually no PMMA dissolved, the final thickness of the gel layer, based on the gel composition, is about three times the initial thickness. The good

agreement between predicted and experimental AC/DC behavior supports the Case II diffusion assumption. Differences in the AC/DC amplitude between Figure 1a and 1b may be attributed to the 2% loss of polymer.

A 1.2 μm PMMA film dissolved completely after four minutes in 80:20 MEK/IPA. The AC/DC trace is shown in Figure 2a. The regular, oscillatory AC/DC behavior is indicative of a constant dissolution rate without significant gel formation. An example of AC/DC indicating gel formation will be presented below. A predicted AC/DC curve for a penetration rate of 310 nm/min, assuming no gel layer is present, is shown in Figure 2b. Also shown are interfacial positions at selected times. The insignificant gel formation and Case II penetration assumptions are supported by the good agreement between Figures 2a and 2b.

The data presented thus far illustrate AC/DC behavior for distinctly different solubility regimes at two selected compositions, that is, complete dissolution in 80:20 MEK/IPA and primarily swelling in 40:60 MEK/IPA. Between these dissolution and swelling regimes, anomalous diffusion was observed over a narrow concentration range. For MEK/IPA at 24.8°C, this narrow transition range (NTR) was found experimentally to extend from 45:55 to 50:50 MEK/IPA. Since it has been shown [23] that polymer solubility decreases with increasing molecular weight(MW) and decreasing temperature, the width and position of this NTR would be expected to be functions of both temperature and polymer MW. To illustrate these effects, ternary phase diagrams will be constructed from polymer phase equilibria theory for different MW's and temperatures.

Phase Equilibria

Given the Flory interaction parameters (χ_{ij}) and the molar volumes (v_i) of nonsolvent, solvent and polymer, a binodal curve of a ternary phase diagram can be constructed by equating the chemical potentials (μ_i) in both phases for each component i [7]. Equations for μ_i in terms of χ_{ij} and v_i are available[7].

Figure 3 is a ternary phase diagram for a nonsolvent(1), solvent(2), polymer(3) system for $\chi_{23}=0$, $\chi_{12}=\chi_{13}=1$, $v_1=v_2=100$ cm^3/mol and polymer MW = $2x10^5$. The selected χ_{ij}'s are approximate values for the IPA/MEK/PMMA system calculated from solubility parameters [8,16,17]. The chosen MW is the measured M_n of the KTI resist.

In Figure 3, points A and B correspond to two hypothetical overall compositions representative of our operating conditions, i.e. polymer fractions of about 10^{-5}. Point A lies within the single phase region, and hence, the resist material dissolves completely into the developer solution (as was seen for 80:20 MEK/IPA). Point B lies within the two phase region. Although not discernible in Figure 3, the calculated polymer fraction in the polymer-poor phase is much less than 10^{-5}. Therefore, this phase would consist overwhelmingly of nonsolvent and solvent. The other phase in equilibrium with B has a composition represented by point B' (located at the opposite end of the tie line). This implies that at a developer composition given by point B, the resist

would not dissolve but, instead, would absorb solvent and nonsolvent from the developer solution until the equilibrium swollen gel composition given by B' is reached. From B', the resulting final thickness of the swollen gel can be calculated assuming the volumes of nonsolvent, solvent and polymer are ideally additive. For the hypothetical point B, this final swollen gel thickness is approximately three times the initial glassy polymer thickness. (This result is similar to that obtained for 40:60 MEK/IPA). When the overall system composition lies near the binodal curve, complex dissolution behavior might be expected. To illustrate this point more clearly, the region enclosed by the dashed lines in Figure 3 is shown in detail in Figures 4 and 5.

Figure 4 shows the binodal curve at very low polymer concentrations for MW's of $2x10^5$ and $5x10^5$ which correspond approximately to M_n and M_w of the KTI resist (χ_{ij} and v_i are the same as for Fig 3). Assuming, for the purpose of discussion, that the resist MW range lies entirely between these two MW's, a developer composition given by point A in Figure 4 would completely dissolve the resist. Likewise, at a developer composition given by point B, the resist would be completely insoluble and swell to an extent dictated by thermodynamics. At developer composition C, however, the lower MW chains in the resist would be soluble while the higher MW chains would be insoluble, thereby fractionating the resist by molecular weight. At equilibrium, the remaining film would be of higher M_n than the starting material. For this particular set of conditions, the NTR would extend only from 46:54 to 47:53 solvent/nonsolvent (see Fig 4). For the idealized case of a

monodisperse polymer (M_w/M_n=1), NTR would shrink to a single composition and the polymer sample would either completely dissolve or remain completely insoluble for any given solvent/nonsolvent composition. The polymer MW range of the KTI resist (M_w/M_n=2.8) obviously extends well above M_w and well below M_n. Hence, the NTR of the KTI resist would be much broader than that indicated in Figure 4. In fact, experimental results have shown the NTR of the KTI resist to be approximately five times greater.

Although not strictly accurate [9,24], χ_{ij} can be assumed to be inversely proportional to temperature as a first approximation [8,25]. Hence, the temperature effect on phase equilibria could be indirectly demonstrated by selecting appropriate χ_{12} values. In this study, the temperature ranged from 24.8°C to 18.4°C. Taking χ_{12} equal to 1.0 at 24.8°C, χ_{12} approximately equals 1.02 at 18.4°C. binodal curves for these χ_{12} values are shown in Figure 5, which is a detailed plot of the same composition region as presented in Figure 4. Here, the binodal curves are drawn for a single MW ($M_n=2\times10^5$) and two different χ_{12}'s ($\chi_{12}=\chi_{13}$, χ_{23}=0 as before).

Consider a developer composition given by point A in Figure 5. At 24.8°C (χ_{12}=1.0), the resist material completely dissolves. At 18.4°C (χ_{12}=1.02), however, this same developer composition would only swell the resist. This sharp transition between total swelling and complete dissolution for such a small temperature change is a direct consequence of the assumed monodisperse nature of the resist for this hypothetical case. For a more realistic case (resist not monodisperse), a band of

binodal curves representing a broader MWD is 'shifted' by a given temperature change (A combination of Figs 4 and 5). If this band of binodal curves is made to pass through the developer composition (by altering the temperature, for instance) varying amounts of polymer will be made soluble or insoluble depending on the relative 'shift' of these curves.

MEK/IPA - Temperature Effect

To investigate the effect of temperature on KTI resist solubility and dissolution behavior in the NTR, samples were immersed in developer compositions of 50:50 MEK/IPA at 24.8°C, 21.7°C and 18.4°C.

At 24.8°C, PMMA dissolved completely in 50:50 MEK/IPA. At 21.7°C, however, 15% of the resist was found to be insoluble and, at 18.4°C, as much as 65% was insoluble. These decreases in solubility due to a decrease in temperature are consistent with the observations in Figures 4 and 5. The fact that the polymer does not completely dissolve is most likely due to the relatively broad MWD of the KTI resist and suggests that the resist material is undergoing MW fractionation due to the relative solubilities of the higher and lower molecular weight polymer chains. For a solvent with marginal dissolution capabilities (e.g., 50:50 MEK/IPA), a decrease in dissolution temperature will cause a greater proportion of the higher MW chains to become insoluble. Therefore, at 18.4°C, the M_n of the polymer remaining on the substrate at equilibrium would be higher than that of the original PMMA sample. At

21.7°C, M_n of the equilibrated film would be even higher. At 24.8°C, the entire range of MW is soluble. The AC/DC curves for these temperatures are shown in Figure 6.

The dissolution behavior observed at 80:20 MEK/IPA is not strictly obeyed for 50:50 MEK/IPA at 21.7°(Fig 6B). Case II swelling appears to dominate during the first five minutes of the run followed by what appears to be nearly 'pure' dissolution. This conclusion is based on the general behavior of the AC/DC signal for the 'pure' swelling and 'pure' dissolution extremes.

Data interpretation for 18.4°C (Fig 6C) is much more difficult due to the numerous oscillations in the AC/DC trace. It should be noted that these oscillations are reproducible from run-to-run. Furthermore, when the sample was left in the solvent for two additional hours, no further gel removal was observed, indicating that equilibrium had been reached after 42 minutes. Based on the data presented thus far, Case II swelling appears to have dominated during the first 12 minutes. Dissolution appears to have dominated between 25 and 42 minutes and would account for about 90% of the PMMA removed during the entire run. Hence, the anomalous behavior between 12 and 25 minutes must be due primarily to swelling effects or large gel composition changes. These observations can be explained in terms of the MW fractionation effect described earlier.

For 50:50 MEK/IPA at 18.4°C, only the lower end of the MWD is soluble. In the initial stages of penetration (0 to 12 min), diffusion

of the lower MW polymer chains is hindered by the presence of the insoluble higher MW chains so relatively little dissolution can occur and therefore, swelling becomes the primary effect observed. After the polymer swells to a sufficient extent (12 min), mobility of the shorter chains is increased. These shorter chains can then migrate to the surface and diffuse into the solvent. Initially this dissolution is slow, resulting in changes in the gel phase composition and, hence, producing 'anomalous' AC/DC behavior (12 to 25 min). At some point (25 min), steady state between penetration and dissolution is reached resulting in 'regular' AC/DC dissolution behavior. After all lower MW chains have diffused into the solvent (42 min), equilibrium is attained and no changes in the AC/DC signal are observed. An insoluble gel layer remains on the substrate surface with a M_n higher than that of the starting material.

MIBK/MeOH - Composition Effect

Experiments similar to those described for MEK/IPA were performed for MIBK/MeOH. Figure 7 shows AC/DC at 24.8°C for 40:60 and 75:25 MIBK/MeOH. These results show Case II behavior similar to the MEK/IPA mixtures; i.e., virtually no dissolution in 40:60 MIBK/MeOH and total dissolution in 75:25 MIBK/MeOH. The NTR occurred between 40:60 and 50:50 MIBK/MeOH which is similar to the NTR found for MEK/IPA. However, unlike MEK/IPA, deviations from standard Case II transport kinetics were observed at MeOH concentrations of 95% and higher. At these MeOH

concentrations, there appeared to be an acceleration of the penetration rate relative to Case II predictions (Super Case II). The details of this accelerated behavior are reported elsewhere [18].

Summary of Kinetics

Figure 8 summarizes the effect of solvent composition on the penetration and dissolution rates of PMMA for MEK/IPA and MIBK/MeOH at 24.8°C. For MEK/IPA (Fig 8a), the penetration rate rises gradually from zero at 100% IPA to about 70 nm/min at the NTR. Above the NTR the penetration rate rises more rapidly to an upper limit of 410 nm/min. There is essentially no dissolution until the NTR is reached. In the NTR, dissolution rises rapidly and becomes equal to the penetration rate. The region enclosed by these two curves represents the solvent composition range in which considerable gel growth is encountered.

MIBK/MeOH (Fig 8b) displays a somewhat different kinetic behavior. Unlike MEK/IPA, there is significant penetration of the pure nonsolvent. This difference is probably due to the smaller size of the MeOH molecule which enables it to pry into the glassy matrix more freely than IPA. The dissolution and penetration rates reach a maximum just above NTR and decrease above about 75% MIBK with pure solvent (100% MIBK) actually yielding the slowest penetration rate. Hence, it can not be assumed that increasing the nonsolvent concentration in the developer solution would necessarily reduce the dissolution rate.

The increase in dissolution rates for intermediate compositions of

MIBK/MeOH may be attributed to the small size of the MeOH molecule which permits rapid penetration. The observed enhancement of penetration rates due to the presence of kinetically mobile species has been observed previously [12].

Summary of Thermodynamics

The effect of developer composition on thermodynamic behavior could be summarized most effectively by representing equilibrium data in a ternary phase diagram. Unfortunately, the psi-meter is incapable of distinguishing the individual concentrations of solvent and nonsolvent in the swollen gel. (The psi-meter 'sees' only their combined swelling effect). However, the amount of polymer in the gel is known (from thickness measurements) and the extent of swelling is calculable (assuming volumes of each component in the gel are ideally additive). Thus, the developer composition effect on swelling can only be summarized in terms of the gel layer polymer fraction, P^*.

A swelling factor, S, can be defined as the ratio of gel thickness at equilibrium (h^*) to initial resist thickness (h_o). Assuming the volumes of polymer, solvent and nonsolvent are ideally additive and no polymer dissolves, S is simply the reciprocal of P^*.

$$S = \frac{h^*}{h_o} = \frac{1}{P^*} \qquad (1)$$

Defining the thermodynamic effect in terms of S is useful for studies

dealing with small geometries such as the features in IC's.

Figure 9 summarizes the effect of developer composition on resist swelling and solubility for MEK/IPA and MIBK/MeOH. For MEK/IPA (Fig 9a), S rises almost linearly from a value of one (no swelling) at 100% IPA to about three at the NTR. Above the NTR, S = 0 since all the polymer dissolves at equilibrium. MIBK/MeOH (Fig 9b) shows a similar trend with S rising from 1.4 at 100% MeOH to about 3 at the NTR.

Figure 9 suggests that for a given developer composition near the NTR in the one phase region, a slight decrease in the relative strength of the developer (e.g. lower solvent to nonsolvent ratio, lower temperature, higher MW resist) may bring about sizable swelling of the resist. In addition, S reaches its maximum value in the NTR, indicating that when this region is crossed, the effect of swelling can be most severe.

CONCLUSIONS

This study demonstrates the usefulness of the psi-meter in determining thermodynamic and kinetic behavior of thin polymeric films in solvent/nonsolvent mixtures. For MEK/IPA, the penetration velocity was constant and could be adequately modeled as Case II transport. The same was true for MIBK/MeOH for MeOH concentrations up to about 95 vol%. For the MEK/IPA system the penetration rate was found to increase with increasing solvent to nonsolvent ratios. However, for MIBK/MeOH, a maximum in penetration rate was observed for an intermediate composition of about 75:25 MIBK/MeOH. This effect was believed to be due to the ability of the relatively small MeOH molecule to penetrate and 'open-up' the polymer network.

The psi-meter also allowed the sharp transition between the thermodynamically controlled swelling and dissolution regimes to be mapped out. At 24.8°C, for both MEK/IPA and MIBK/MeOH, this transition occurred at about 50:50 solvent/nonsolvent. At this composition, a decrease in temperature caused greater insolubility over a wider range of MW. This fractionation was believed to yield insoluble films of higher M_n than the original polymer. During fractionation, AC/DC data suggested a period of initial swelling followed by anomalous behavior and finally, dissolution. This induction period for dissolution was attributed to hindered diffusion of the soluble, shorter polymer chains due to the presence of insoluble, longer chains.

ACKNOWLEDGMENT

This project was supported by the Air Force Office of Scientific Research under Grant AFOSR-90-0078.

REFERENCES

1. D.J. Elliot, Integrated Circuit Fabrication Technology, McGraw-Hill Book Company, New York, 1982, p. 209.

2. F. Asmussen and K. Ueberreiter, J. Polym. Sci., 57, 199 (1962).

3. D.W. van Krevelen, Properties of Polymers, Elsevier Scientific Publishing Co., Amsterdam, 1976, p. 141.

4. F.W. Billmeyer, Textbook of Polymer Science, Wiley-Interscience, New York, 1984, p. 153.

5. C.M. Hansen, J. Paint Technol., 39, 104 (1967).

6. A.F.M. Barton, Handbook of Solubility Parameters and Other Cohesion Parameters, CRC Press, Inc., Boca Raton, Fl, 1983, p. 141.

7. P.J. Flory, Principles of Polymer Chemistry, Cornell University Press, Ithaca, New York, 1953, p. 548.

8. J.M. Prausnitz, Molecular Thermodynamics of Fluid-Phase Equilibria, Prentice-Hall, Englewood Cliffs, New Jersey, 1969, p. 297.

9. J. Brandrup and E.H. Immergut, eds., Polymer Handbook, Wiley, New York, 1975, p. IV-131.

10. D.W. van Krevelen, Properties of Polymers, Elsevier Scientific Publishing Co., Amsterdam, 1976, p. 143.

11. N. Thomas and A.H. Windle, Polymer, 19, 255 (1978).

12. F. Rodriguez, P.D. Krasicky, and R.J. Groele, Solid State Technol., 28(5), 125 (1985).

13. T.A. Alfrey, E.F. Gurnee, and W.G. Lloyd, J. Polym. Sci. (C), 12, 249 (1966).

14. N.L. Thomas and A.H. Windle, Polymer, 21, 613 (1980).

15. B. Wu, MS Thesis, University of California, Berkeley, December 1982.

16. A.F.M. Barton, Handbook of Solubility Parameters and Other Cohesion Parameters, CRC Press, Inc., Boca Raton, Fl, 1983, p. 94.

17. J.M. Prausnitz, Molecular Thermodynamics of Fluid-Phase Equilibria, Prentice-Hall, Englewood Cliffs, New Jersey, 1969, p. 298.

18. J. Manjkow, MS Thesis, University of California, Berkeley, December 1986.

19. W.W. Flack, J.S. Papanu, D.W. Hess, D.S. Soong, and A.T. Bell, J. Electrochem. Soc., 131, 2200 (1984).

20. W.W. Flack, PhD Dissertation, University of California, Berkeley, December 1983.

21. A. Zaghloul and R. Azzam, Surface Sci., 96, 169 (1980).

22. F.L. McCrackin, National Bureau of Standards, Technical Note 479 (1969).

23. J.H. Lai and L. Shepherd, J. Appl. Polym. Sci., 20, 2367 (1976).

24. P.J. Flory, Principles of Polymer Chemistry, Cornell University Press, Ithaca, New York, 1953, p. 545.

25. J.M. Prausnitz, Molecular Thermodynamics of Fluid-Phase Equilibria, Prentice-Hall, Englewood Cliffs, New Jersey, 1969, p. 272.

FIGURE CAPTIONS

Figure 1. a) AC/DC data for PMMA in 40:60 MEK/IPA at 24.8°C. b) Predicted AC/DC behavior assuming Case II transport with no dissolution for a gel composition of 36% PMMA and a penetration rate of 43.5 nm/min. Relative positions of the solvent/gel and gel/glass interfaces are shown for selected times.

Figure 2. a) AC/DC data for PMMA in 80:20 MEK/IPA at 24.8°C. b) Predicted AC/DC behavior assuming Case II transport with no significant gel formation and a penetration velocity of 310 nm/min. Relative positions of the solvent/glass interface are shown for selected times.

Figure 3. Ternary phase diagram for a nonsolvent(1), solvent(2), polymer(3) system taking $\chi_{23} = 0$ and $\chi_{12} = \chi_{13} = 1.0$; MW = 2×10^5. (The region enclosed by the dashed lines is shown in detail in Figures 4 and 5).

Figure 4. Detail of Figure 3 for $\chi_{12} = 1.0$ and polymer molecular weights of 2×10^5 and 5×10^5. These values are the approximate M_n and M_w of the KTI Resist. ($\chi_{13} = \chi_{12}$, $\chi_{23}=0$ as in Figure 3).

Figure 5. Detail of Figure 3 for a polymer molecular weight of 2×10^5 and χ_{12} equal to 1.0 and 1.02. For $\chi_{12} = 1.00$ at 24.8°C, $\chi_{12} \approx 1.02$ at 18.4°C assuming all other parameters are held constant. ($\chi_{13} = \chi_{12}$, $\chi_{23} = 0$ as in Figure 3).

Figure 6. AC/DC data for PMMA in 50:50 MEK/IPA at a) 24.8°C, b) 21.7°C, and c) 18.4°C.

Figure 7. AC/DC data at 24.8°C for PMMA in a) 40:60 MIBK/MeOH and b) 75:25 MIBK/MeOH.

Figure 8. Penetration and dissolution rates of PMMA as a function of solvent concentration at 24.8°C for a) MEK/IPA and b) MIBK/MeOH.

Figure 9. Swell factor (S) as a function of solvent concentration at 24.8°C for a) MEK/IPA and b) MIBK/MeOH. S is the ratio of the gel thickness at equilibrium to the initial PMMA thickness (1.2 μm).

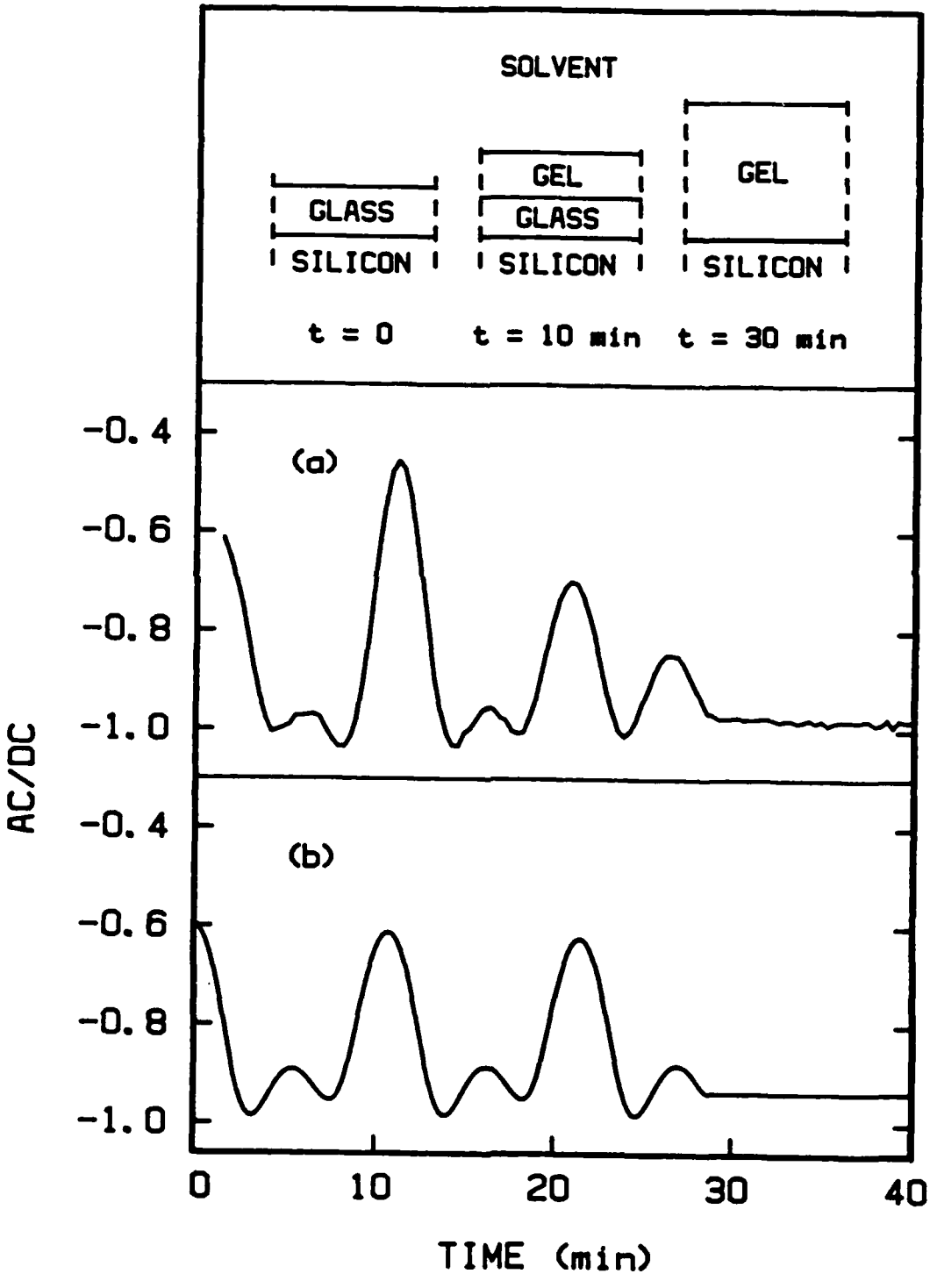
SOLVENT
GLASS
SILICON
GEL
GLASS
SILICON
GEL
SILICON
t = 0
t = 10 min
t = 30 min
(a)
(b)
-0.4
-0.6
-0.8
-1.0
AC/DC
0
10
20
30
40
TIME (min)

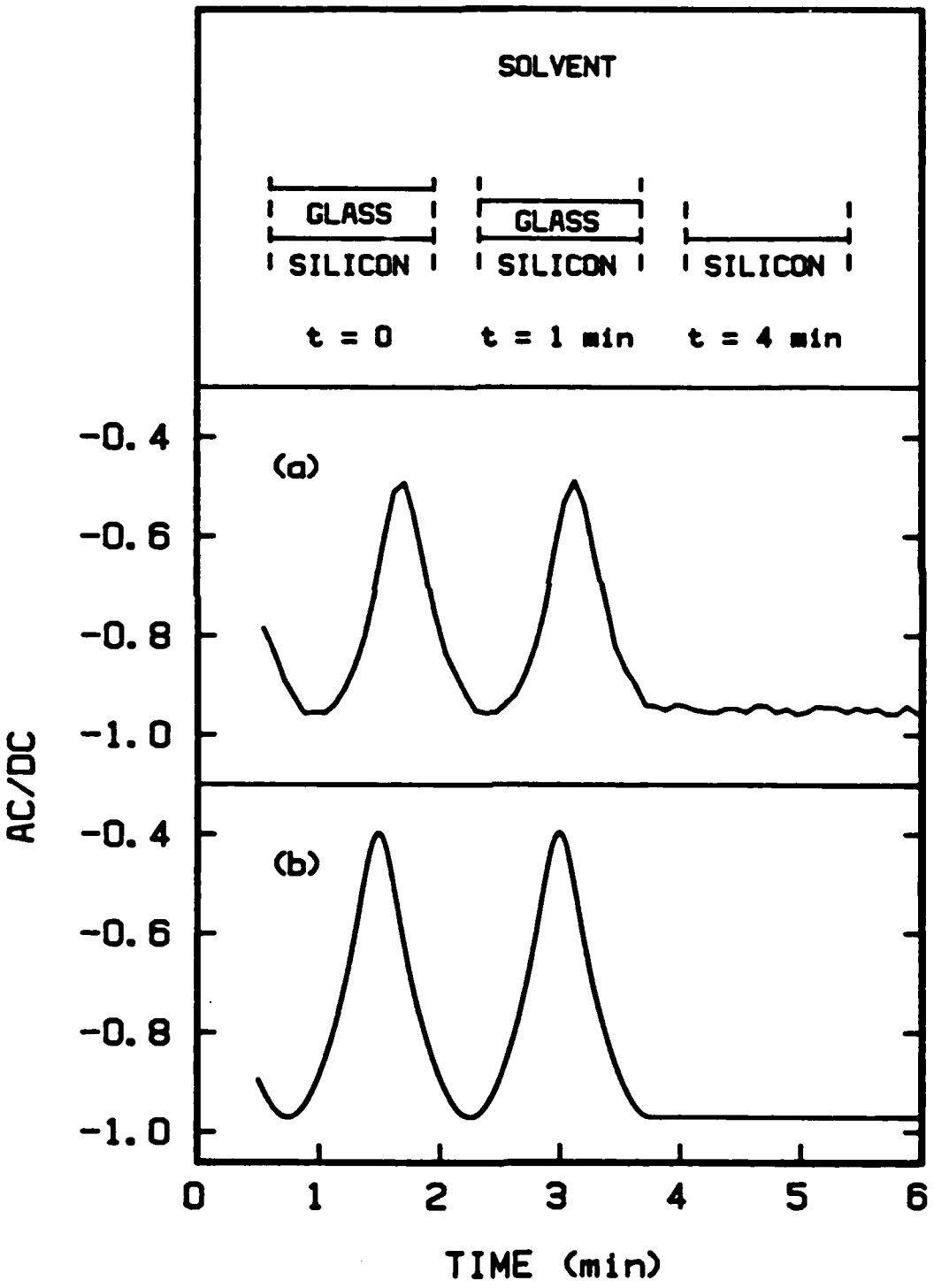
SOLVENT
GLASS
SILICON
GLASS
SILICON
SILICON
t = 0
t = 1 min
t = 4 min
(a)
(b)
-0.4
-0.6
-0.8
-1.0
-0.4
-0.6
-0.8
-1.0
AC/DC
0
1
2
3
4
5
6
TIME (min)

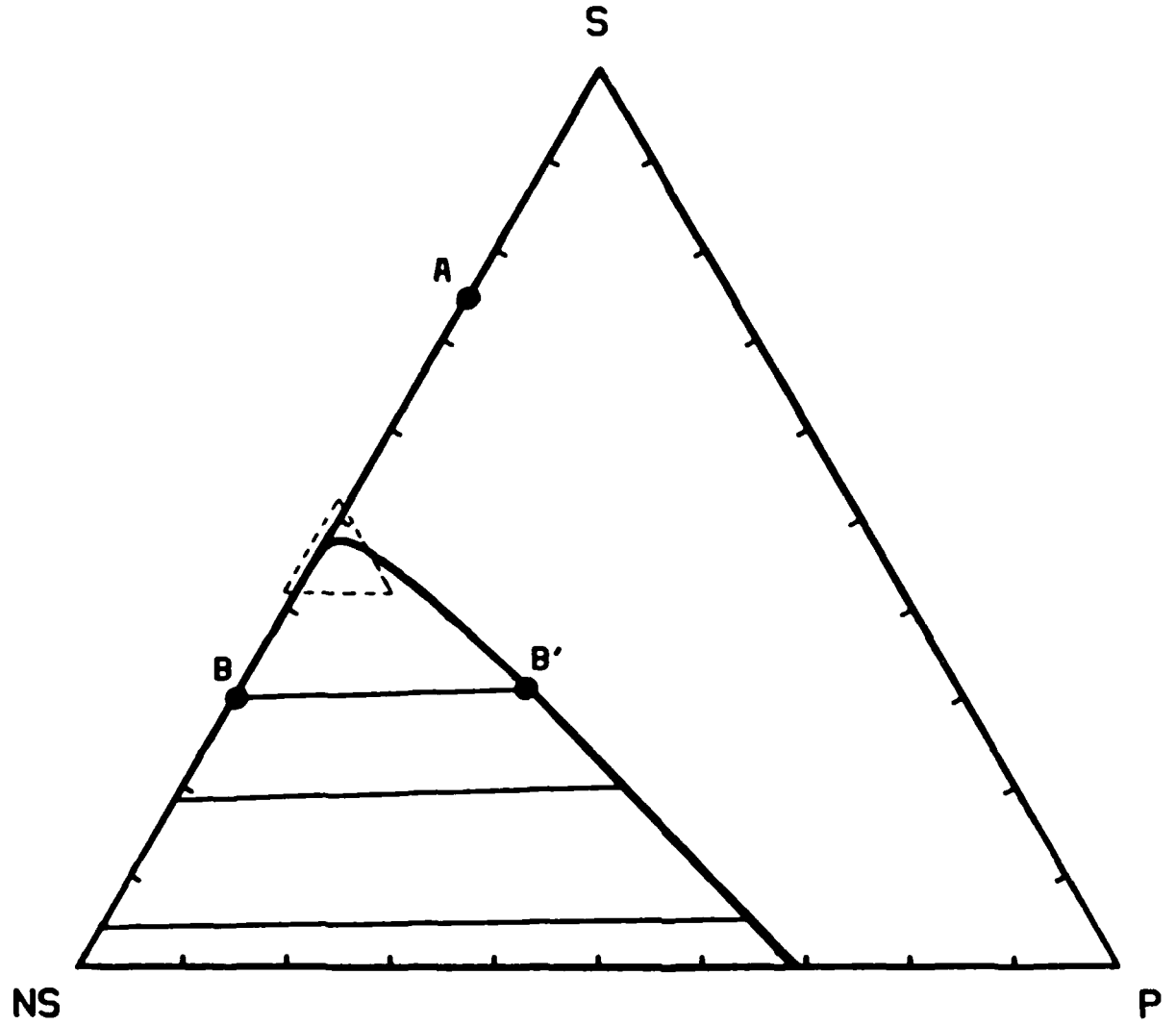
S
A
B
B'
NS
P

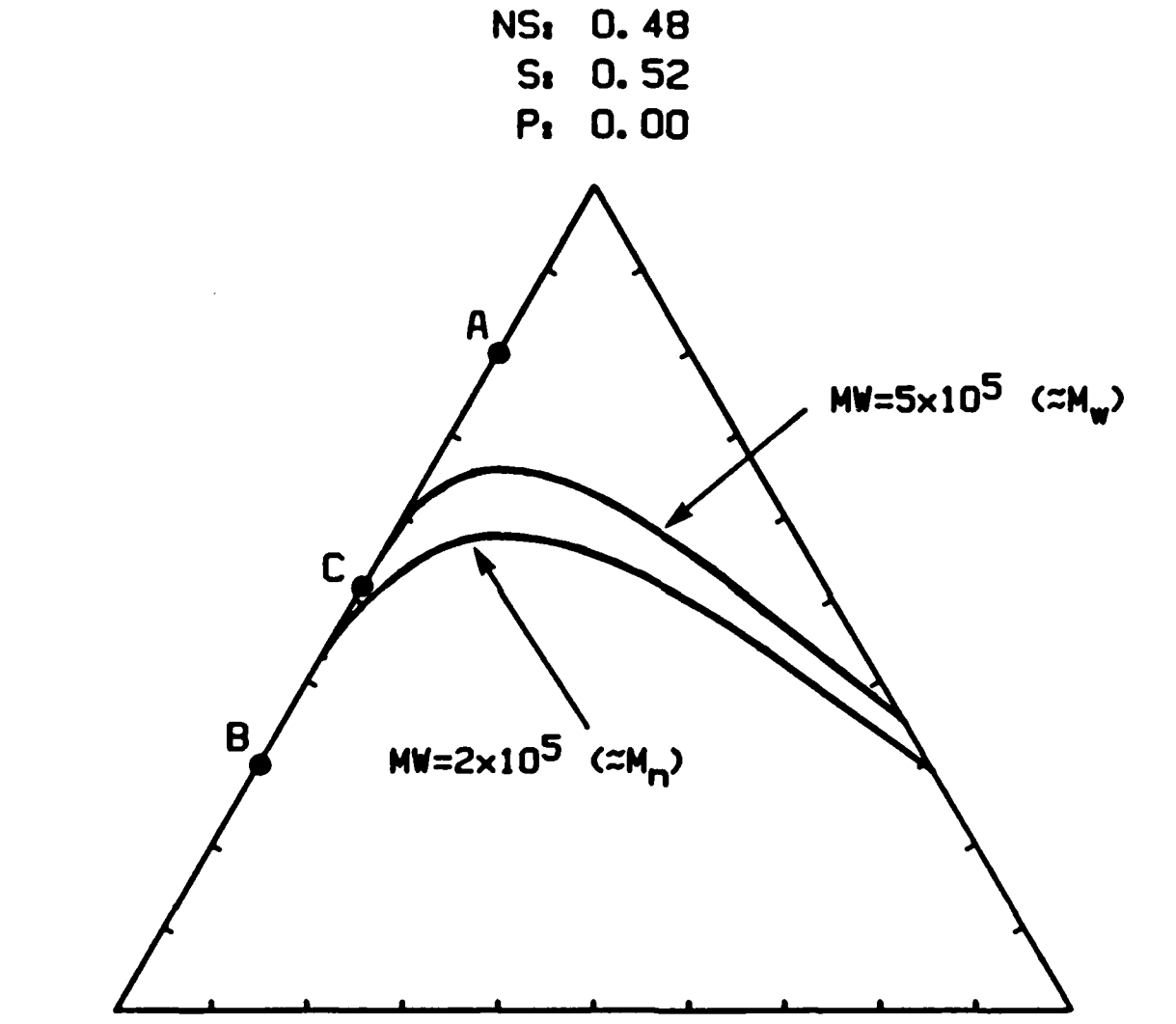
NS: 0.48
S: 0.52
P: 0.00
A
C
B
MW=5x10^5 (≈M_w)
MW=2x10^5 (≈M_n)
NS: 0.58
S: 0.42
P: 0.00
NS: 0.48
S: 0.42
P: 0.10

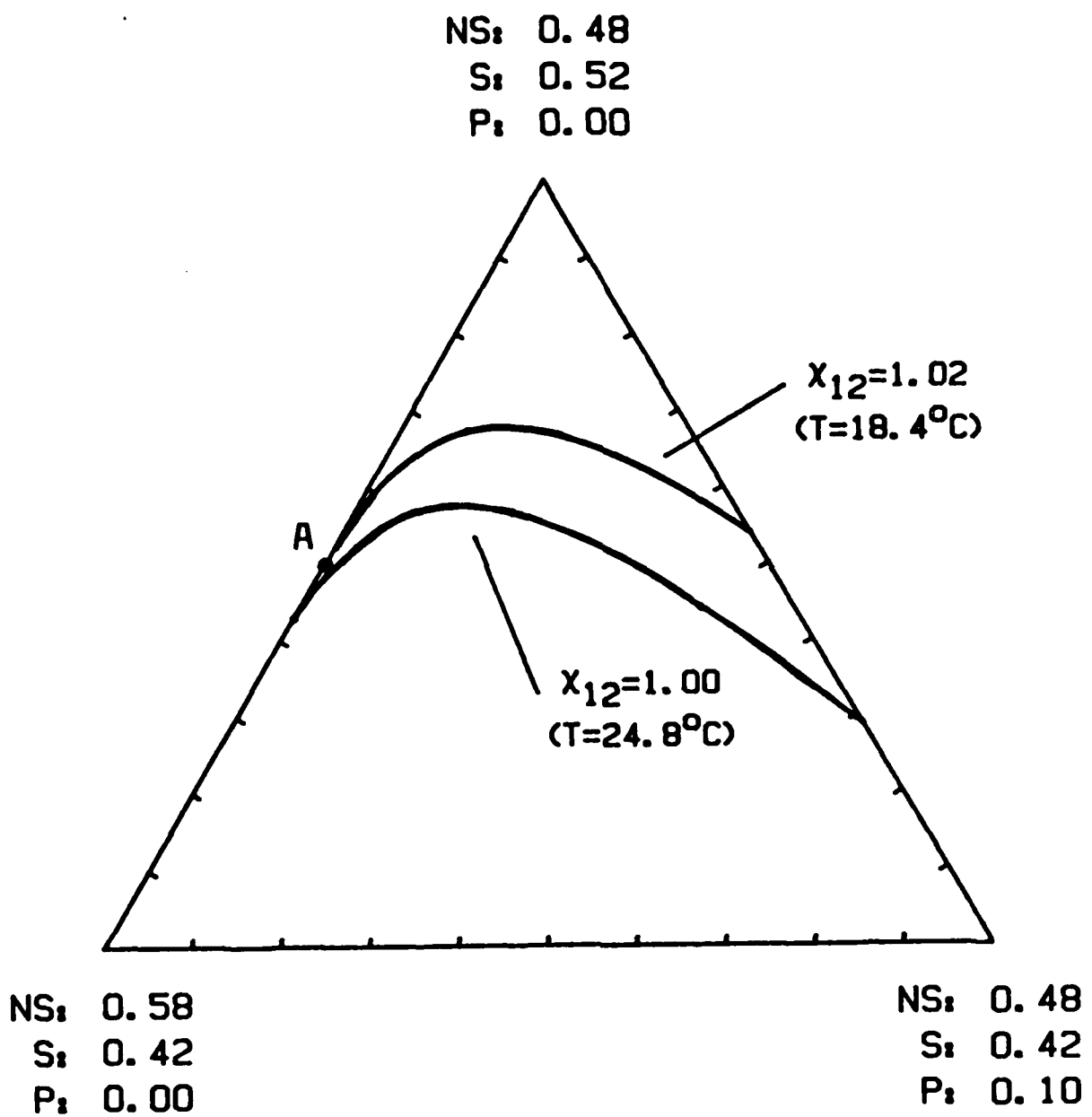
NS: 0.48
S: 0.52
P: 0.00
X_{12}=1.02
(T=18.4°C)
A
X_{12}=1.00
(T=24.8°C)
NS: 0.58
S: 0.42
P: 0.00
NS: 0.48
S: 0.42
P: 0.10

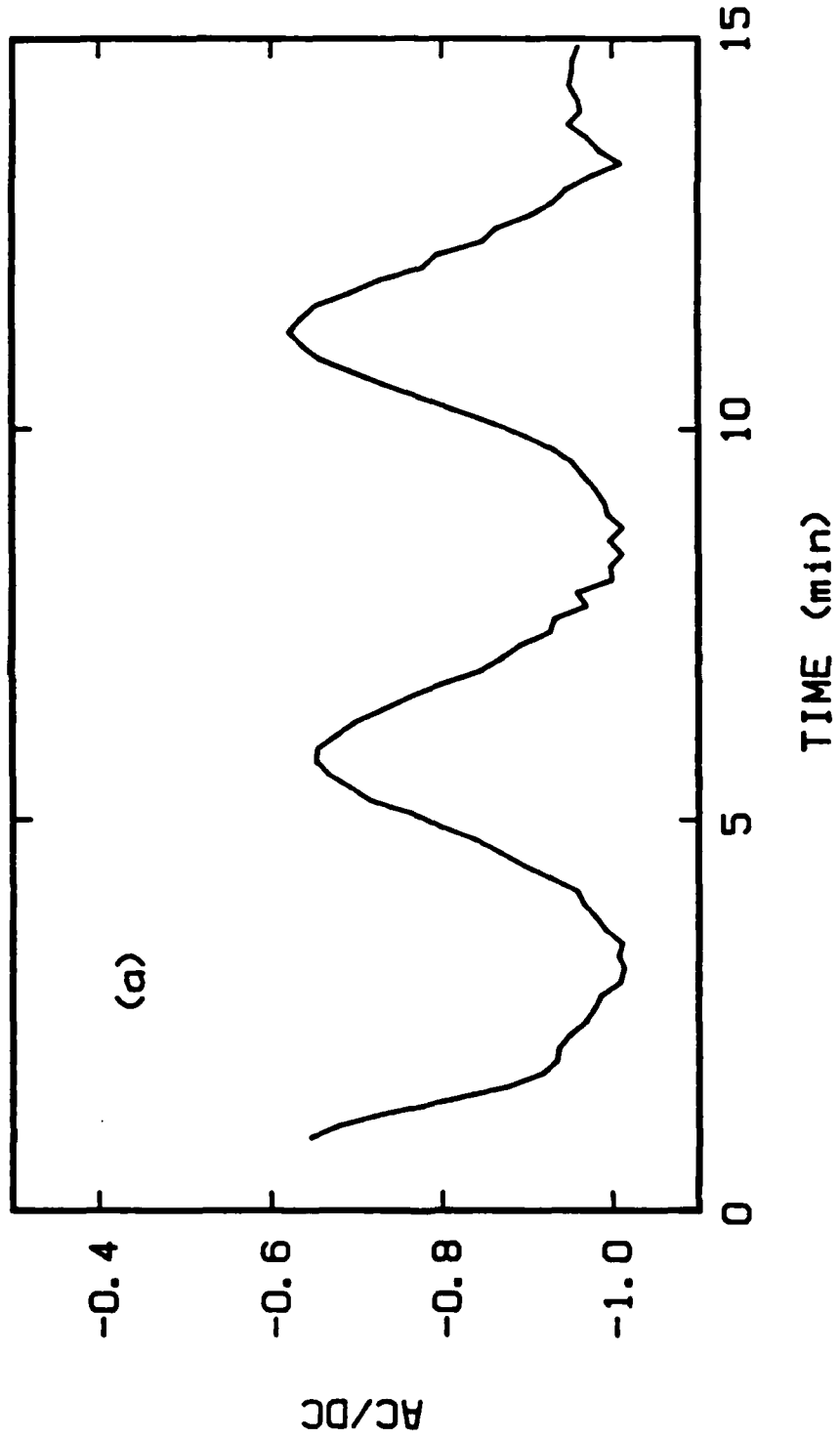
AC/DC
-0.4
-0.6
-0.8
-1.0
0
5
10
15
TIME (min)
(a)

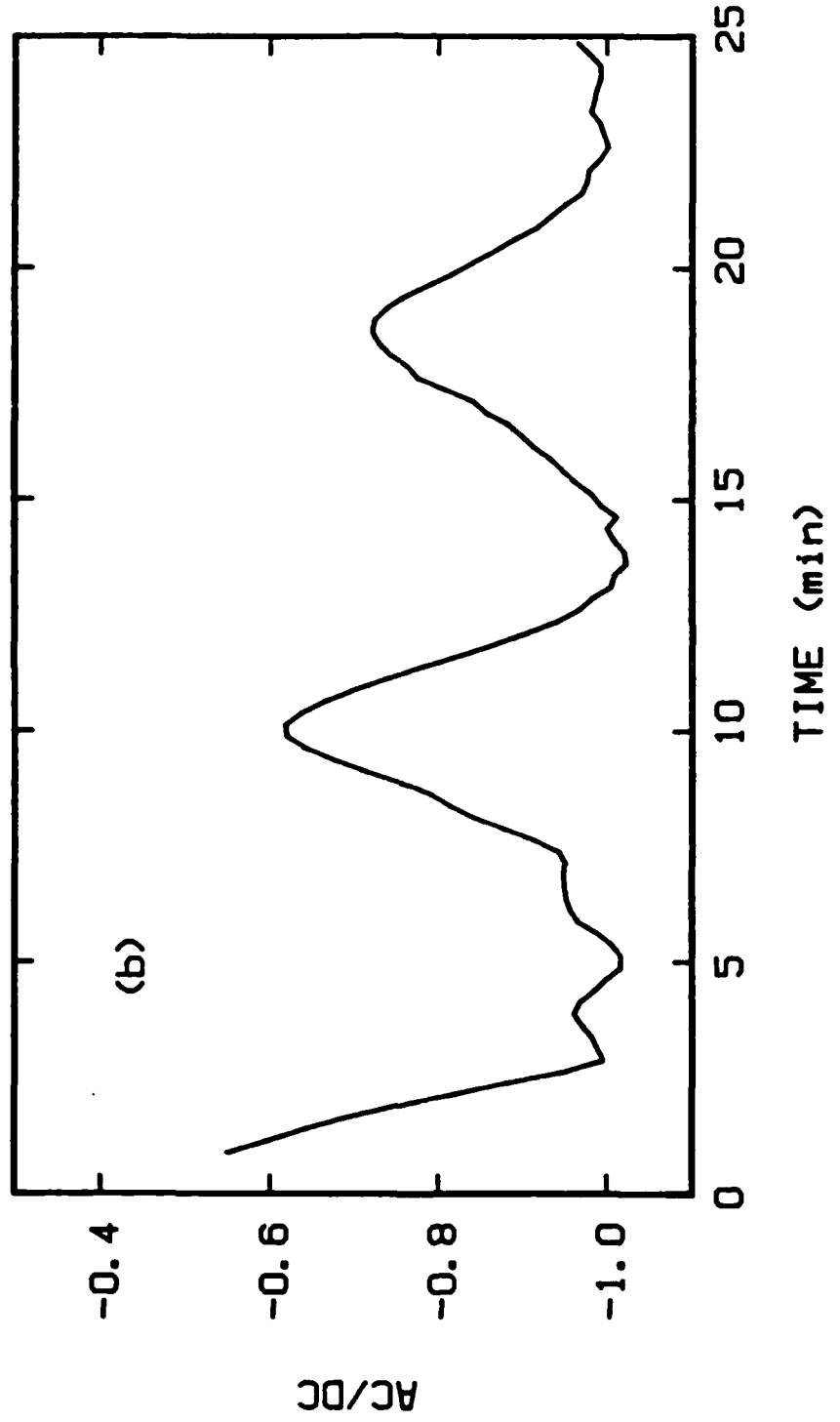
(b)
AC/DC
-0.4
-0.6
-0.8
-1.0
0
5
10
15
20
25
TIME (min)

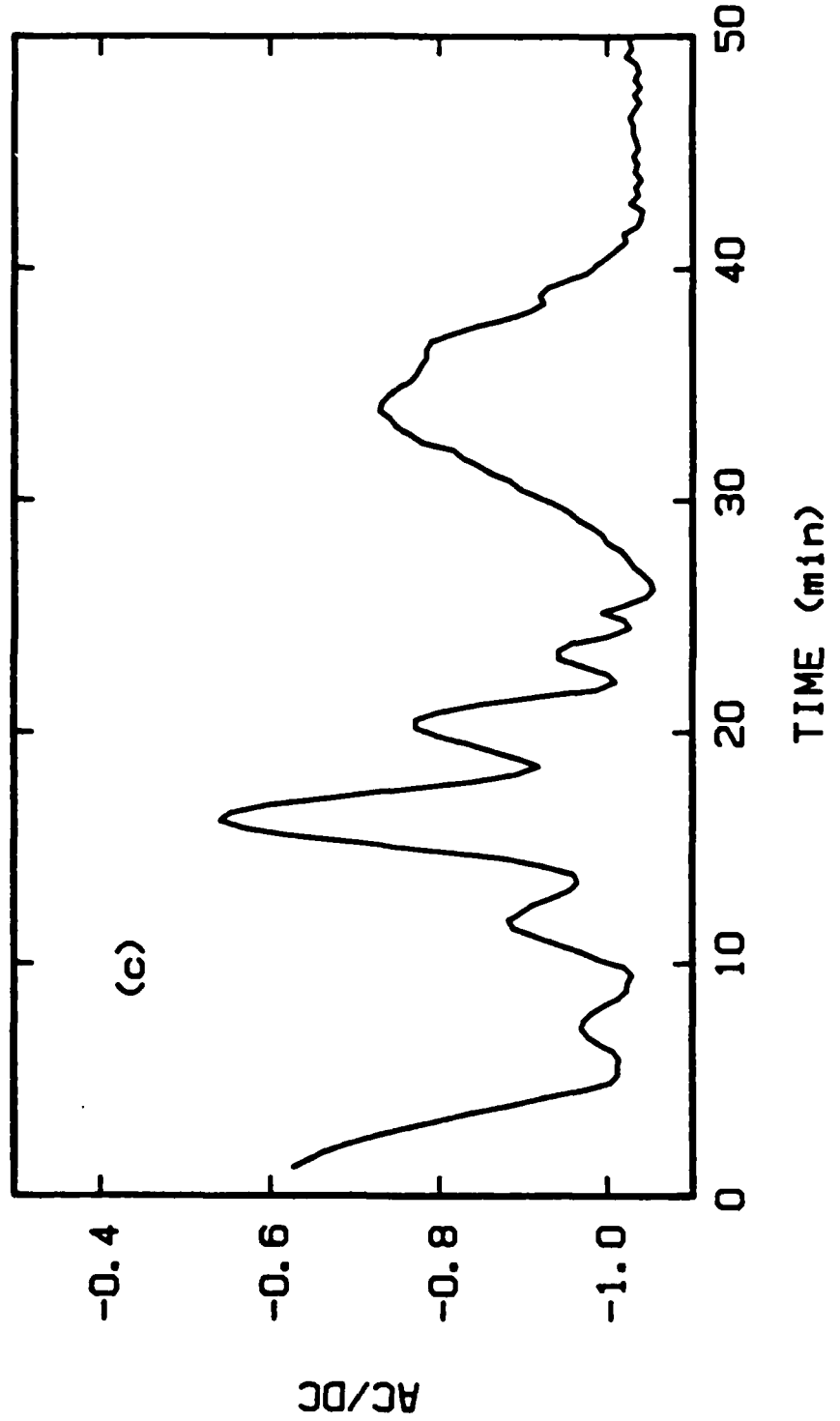
(c)
AC/DC
-0.4
-0.6
-0.8
-1.0
0
10
20
30
40
50
TIME (min)

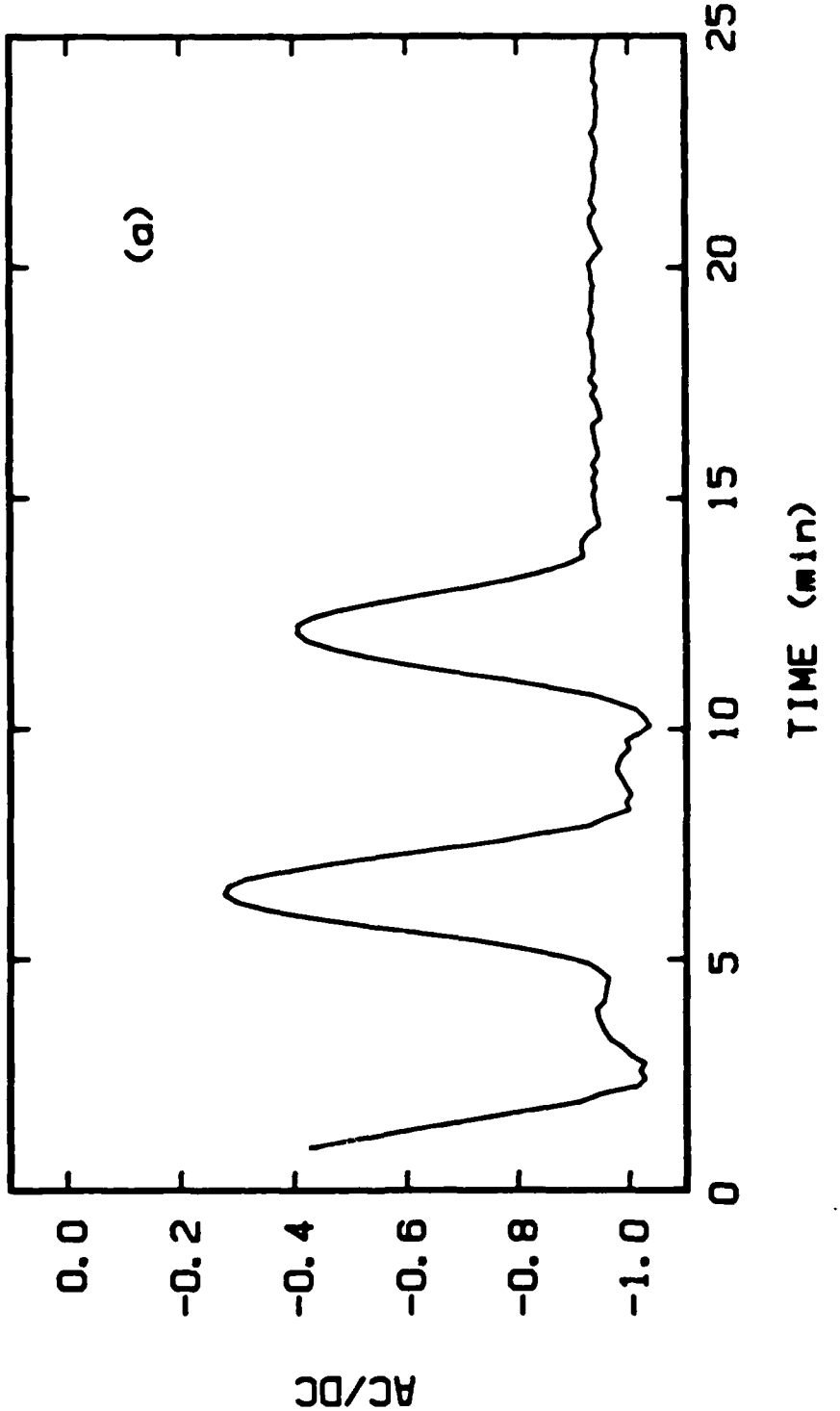
(a)
AC/DC
0.0
-0.2
-0.4
-0.6
-0.8
-1.0
0
5
10
15
20
25
TIME (min)

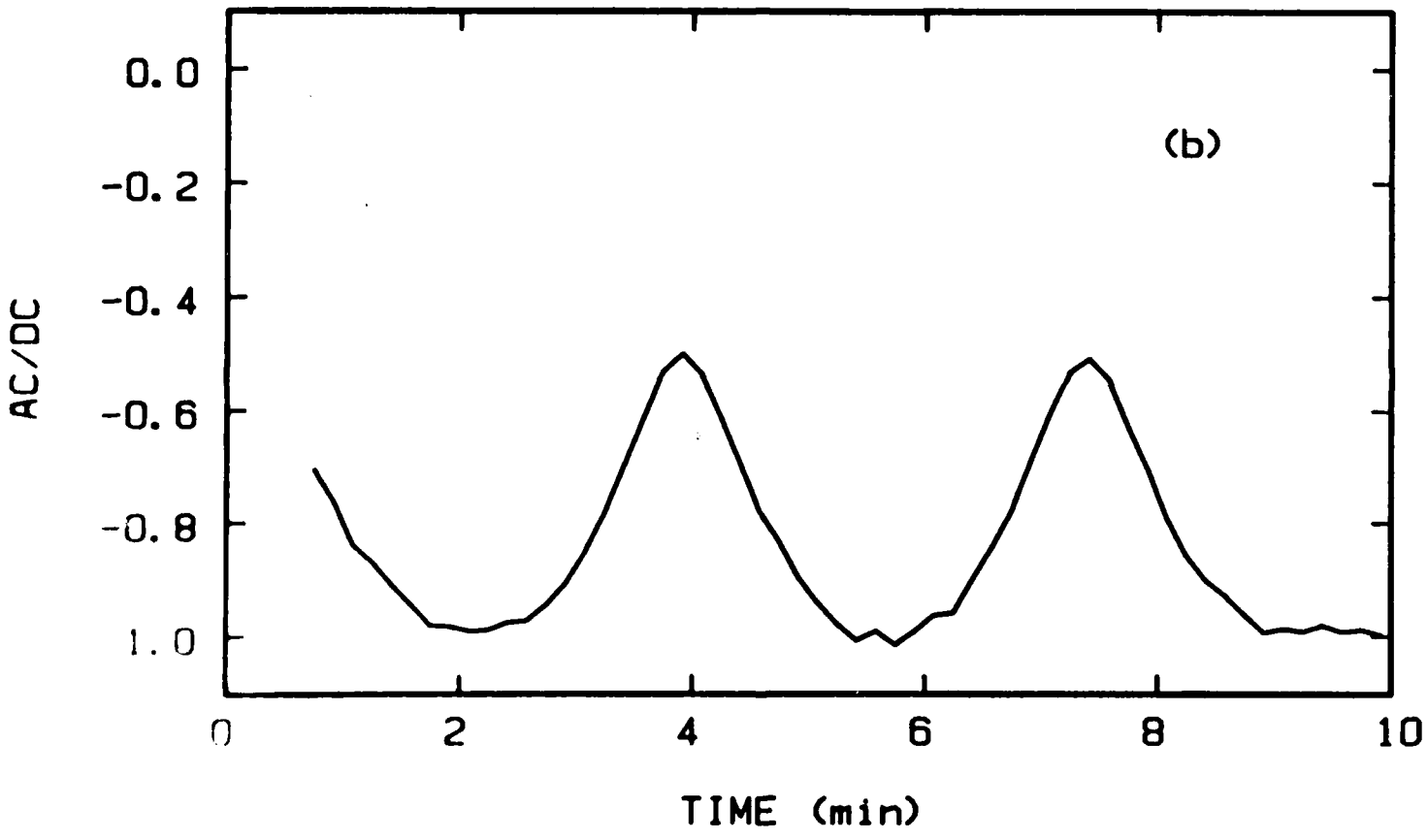
0.0
-0.2
-0.4
-0.6
-0.8
1.0
AC/DC
(b)
0
2
4
6
8
10
TIME (min)

AD-A179 499 CONTINUATION OF RESEARCH IN THE DEVELOPMENT OF HIGH SENSITIVITY X-RAY AND (U) CALIFORNIA UNIV BERKELEY ELECTRONICS RESEARCH LAB A BELL ET AL 25 FEB 87 2/2

UNCLASSIFIED AFOSR-TR-87-0380 AFOSR-85-0084 F/G 13/8 NL

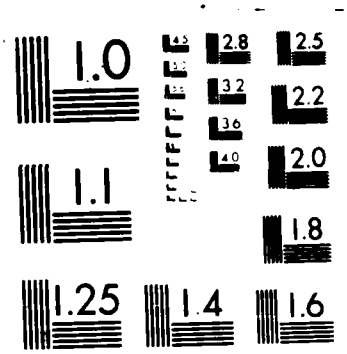

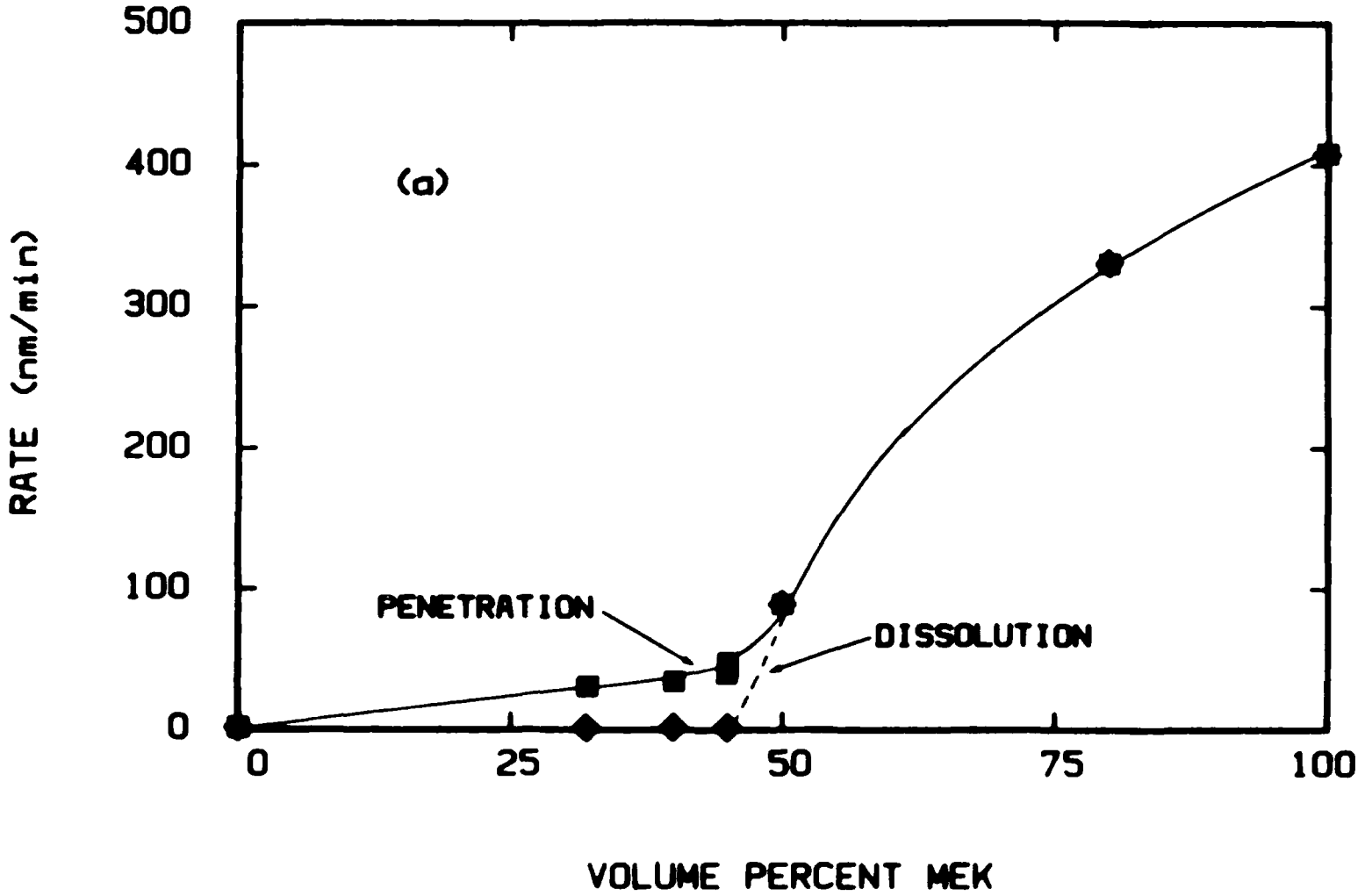
500
400
300
200
100
0
RATE (nm/min)
(a)
PENETRATION
DISSOLUTION
0
25
50
75
100
VOLUME PERCENT MEK

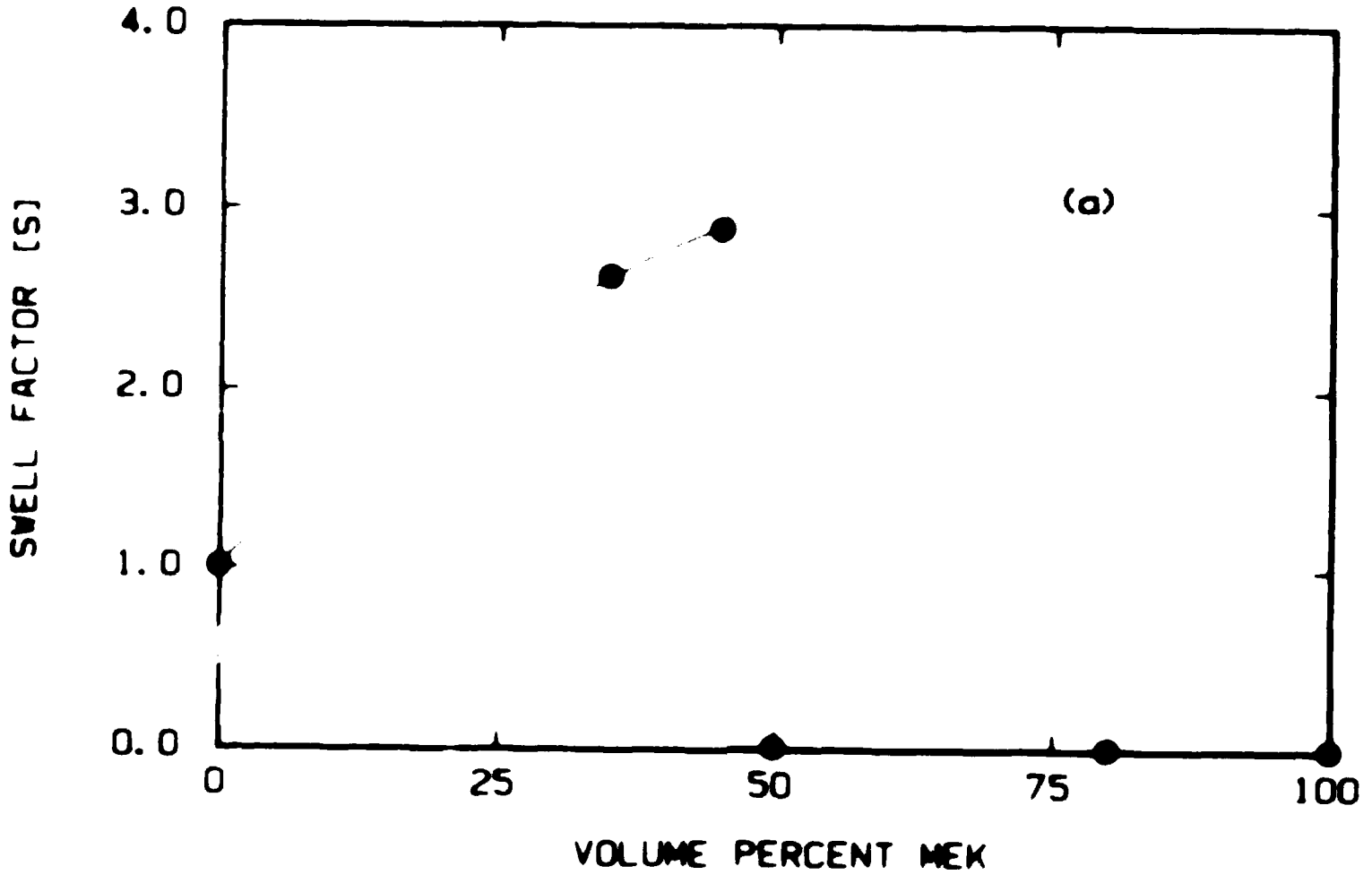
4.0
3.0
2.0
1.0
0.0
SWELL FACTOR [S]
(a)
0
25
50
75
100
VOLUME PERCENT MEK

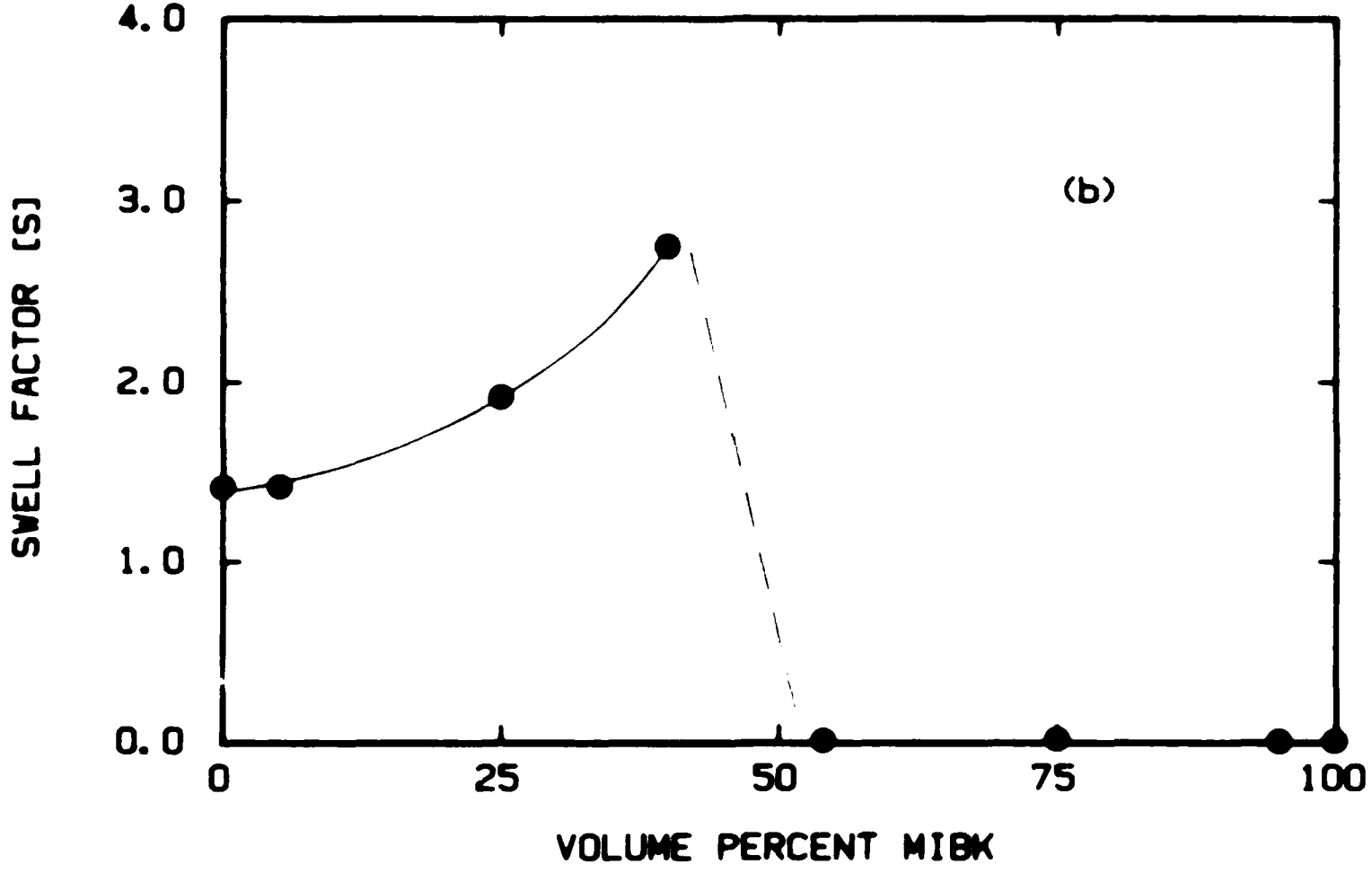
4.0
3.0
2.0
1.0
0.0
SWELL FACTOR [S]
(b)
0
25
50
75
100
VOLUME PERCENT MIBK

END

5-87

DTIC